Efficacy of NEDD8 Pathway Inhibition in Preclinical Models of Poorly Differentiated, Clinically Aggressive Colorectal Cancer

Picco, Gabriele; Petti, Consalvo; Sassi, Francesco; Grillone, Katia; Migliardi, Giorgia; Rossi, Teresa; Isella, Claudio; Di Nicolantonio, Federica; Sarotto, Ivana; Sapino, Anna; Bardelli, Alberto; Trusolino, Livio; Bertotti, Andrea; Medico, Enzo. Efficacy of NEDD8 Pathway Inhibition in Preclinical Models of Poorly Differentiated, Clinically Aggressive Colorectal Cancer. JOURNAL OF THE NATIONAL CANCER INSTITUTE. 109 (2) pp: 1-12.
DOI: 10.1093/jnci/djw209

JNCI 16-0258R1 - Postprint

Article

Efficacy of NEDD8 pathway inhibition in preclinical models of poorly differentiated, clinically aggressive colorectal cancer.

Authors: Gabriele Picco[1,2], Consalvo Petti[1,2], Francesco Sassi[2], Katia Grillone[2], Giorgia Migliardi[2], Teresa Rossi[2], Claudio Isella[1,2], Federica Di Nicolantonio[1,2], Ivana Sarotto[1], Anna Sapino[1,3], Alberto Bardelli[1,2], Livio Trusolino[1,2], Andrea Bertotti[1,2] and Enzo Medico*[1,2]

Affiliations:

[1]Candiolo Cancer Institute – FPO IRCCS, SP 142, Km 3.95, 10060 Candiolo, Torino, Italy

[2]University of Torino, Department of Oncology, SP 142, Km 3.95, 10060 Candiolo, Torino, Italy

[3]University of Torino, Department of Medical Sciences, Corso Bramante, 88 Torino, Italy

*Corresponding author

Candiolo Cancer Institute, Strada Prov. 142, km 3,95 – 10060 Candiolo (TO)

e-mail: enzo.medico@unito.it

Abstract:

Background. The NEDD8 conjugation pathway modulates the ubiquitination and activity of a wide range of intracellular proteins, and its blockade by pevonedistat is emerging as a promising therapeutic approach in various cancer settings. However, systematic characterization of pevonedistat efficacy in specific tumor types and definition of response predictors are still missing.

Methods. We investigated *in vitro* sensitivity to pevonedistat in 122 colorectal cancer (CRC) cell lines by an ATP-based proliferation assay, and evaluated apoptosis and DNA content by flow cytometry. Associations between pevonedistat sensitivity and CRC molecular features were assessed by Student's t test. A 184-gene transcriptional predictor was generated in cell lines and applied to 87 metastatic CRC samples for which patient-derived xenografts (PDXs) were available. *In vivo* reponse to pevonedistat was assessed in PDX models (≥ 5 mice per arm). All statistical tests were two-sided.

Results. Sixteen (13.1%) cell lines displayed a marked response to pevonedistat, featuring DNA re-replication, proliferative block, and increased apoptosis. Pevonedistat sensitivity did not statistically significantly correlate with microsatellite instability or mutations in *KRAS* or *BRAF*, and was functionally associated with low EGFR pathway activity. While ineffective on predicted resistant PDXs, *in vivo* administration of pevonedistat statistically significantly impaired growth of five out of six predicted sensitive models ($P < .01$). In samples from CRC patients, transcriptional prediction of pevonedistat sensitivity was associated with poor prognosis after surgery ($P = .003$, HR = 2.49, 95% CI = 1.34 to 4.62) and early progression under cetuximab treatment ($P < .001$, HR = 3.59, 95% CI = 1.60 to 8.04). Histological and immunohistochemical analyses revealed that the pevonedistat sensitivity signature captures transcriptional traits of poor differentiation and high-grade mucinous adenocarcinoma.

Conclusion. These results highlight NEDD8-pathway inhibition by pevonedistat as a potentially effective treatment for poorly differentiated, clinically aggressive CRC.

Introduction

Each year, approximately 700,000 new cases of CRC are diagnosed worldwide, and of these 60% develop metastatic disease (1). In addition to chemotherapy, inhibition of the epidermal growth factor receptor (EGFR) has been successfully deployed for treatment of CRC (2, 3). However, EGFR-targeted therapy is ineffective in more than 80% of the cases, due to molecular alterations of downstream signal transducers, like KRAS, BRAF, and NRAS (4-6), and to additional resistance mechanisms (7). Alternative targeted therapies for CRC have been focused at inhibition of kinases in the same pathway, including HER2, TRK, ALK, IGFR, BRAF, and MEK, resulting in a narrow spectrum of activity (8, 9). As a consequence, there is an unmet need for therapies targeting alternative pathways in CRC.

As an attractive option we considered blockade of the NEDD8 conjugation pathway. The NEDD8 gene (neural precursor cell-expressed developmentally downregulated 8) encodes a ubiquitin-like protein that, similarly to ubiquitin, acts by a covalent conjugation process ('neddylation") that involves its transfer to specific target proteins (10, 11). NEDD8 conjugation proceeds through a sequence initiated by its activation by the E1 protein complex, composed of the NEDD8 activating Enzyme 1 (NAE1) and UBA3 gene products, followed by its transfer to the E2 enzyme UBE2M, and finally to substrate conjugation via a series of E3 ligases (12). Intriguingly, the best-characterized proteins activated by neddylation are cullins 1 to 9, which are regulatable scaffolds of the family of E3 ubiquitin-ligases, known as cullin-RING ligases (CRLs) (13). Neddylated CRLs ubiquitinate specific sets of substrates involved in cell cycle, transcription, signal transduction, and development (12). Moreover, direct neddylation occurs on proteins with an established role in cancer, like MDM2, EGFR, HIFα, and VHL (11). Therefore, by modulating protein stability or activity, neddylation can play a key role in the control of cancer cell proliferation and apoptosis (14, 15).

For these reasons, inhibition of the NEDD8 conjugation pathway has been recently explored as a candidate therapy for cancer. Pevonedistat (MLN4924), a first-in class selective inhibitor of UBA3, showed remarkable activity in cell lines from multiple myeloma and various epithelial cancers (16-19). In sensitive cells, pevonedistat was found to induce DNA rereplication, apoptosis and senescence (20-23). In phase I clinical trials for hematological and solid neoplasms, pevonedistat was effective in a subset of cases, highlighting the need of predictive biomarkers (24-26). Indeed, the limited number of preclinical models and patients tested for each cancer type prevented evaluation of response predictors.

To evaluate the spectrum of activity of pevonedistat in CRC, and to define possible response predictors, we therefore exploited a large collection of molecularly profiled CRC cell lines and patient-derived xenografts (PDXs), reliably representing the molecular heterogeneity of the disease (7, 9, 27). Pevonedistat testing on 122 CRC cell lines enabled the construction of a transcriptional response predictor, that was then prospectively validated *in vivo* using PDXs from metastatic CRC.

Materials and Methods

Cell lines and drugs

From a collection of 151 CRC cell lines (9), a panel of 122 genetically unique models were tested for *in vitro* sensitivity to pevonedistat at concentrations ranging from 1nM to 10μM. Cell lines were cultured as specified in **Supplementary Table 1**. Cell lines of the HROC series (28-30) were obtained from Michael Linnebacher (University of Rostock, Rostock, Germany) For in vitro experiments pevonedistat (MLN4924) was obtained from Active Biochem (CAT#: A-1139, Maplewood, NJ). For in vivo studies the compound was provided by Millennium Pharmaceuticals, Inc. (Cambridge, MA).

Gene expression data analysis

Gene expression data from the 122 CRC cell lines were extracted from the Gene Expression Omnibus (GEO, accession: GSE59857; **Supplementary Table 1**), normalized and preprocessed (expression filtering, removal of redundant probes, log_2 transformation, log_2ratio vs. average) as previously described (9). To construct a transcriptional predictor of response to pevonedistat, log_2signal values in the 16 sensitive and 44 resistant cells were compared by t-test ($P < .001$ and > 1.7 fold-change (absolute log2 ratio). False discovery rate (FDR) analysis was performed by Monte Carlo simulation considering 2,000 random sample permutations. The fraction of false positive hits was very low (1.56 %). The expression of the signature genes was visualized by the GEDAS software 1.1.6 Beta (31). Gene expression data from 87 CRC-LM samples for which PDX derivatives were extracted from a 185 CRC-LM GEO dataset (Isella et al., manuscript submitted; GSE73255). Expression filtering was performed selecting probes detected in at least one sample. Among redundant probes, the probe with the highest average value was selected for further analysis. For survival analysis, gene expression profiles from 290 primary CRC surgical specimens were downloaded from GEO (GSE14333) (32). For progression-free survival analysis, gene expression data of metastatic CRC samples were downloaded from GEO (GSE5851) and 61 LM-CRC were exploited for further analysis (33).

Statistical analyses

All experimental error bars display standard deviation. All tests were two-sided, and P values of less than .05 were considered statistically significant. For comparison between pevonedistat treated and vehicle-treated PDX tumor volumes were compared at experimental endpoint by two-tailed t tests. Statistical significance of Pearson correlations were evaluated by the "SISA" web-based tool, available at http://www.quantitativeskills.com/sisa/statistics/correl.htm (Accessed: 2015, May 25). Cox regression hazard and Kaplan-Meier analyses were conducted with the R Bioconductor 'survival'

package (34). Assumption of proportionality for Cox proportional hazards was evaluated with the function cox.zph in all the analyses carried out. Statistics were run as a computational pipeline on the entire data set so that the investigator had no direct view of the single-case outcome or of its prediction. Linear regression analysis was performed in R with the *glm* function according to default parameters.

Human tumor samples and animal studies

All patients (n=87) provided written informed consent and samples were procured and the study was conducted under the approval of the Review Boards of the Candiolo Cancer Institute. Clinical and pathologic data were entered and maintained in our prospective database. Female 6-week-old NOD-SCID mice (Charles River Laboratories, Wilmington, MA) were used in the xenograft and PDX in vivo studies. All animal procedures were approved by the Ethical Commission of the Candiolo Cancer Institute and by the Italian Ministry of Health.

Further details on experimental procedures and data analysis are provided in the **Supplementary Methods**.

Results

Effects of NEDD8-pathway inhibition by pevonedistat on CRC cell lines

Of 122 tested CRC cell lines, 16 (13.1%) displayed marked *in vitro* sensitivity to pevonedistat (**Figure 1A**; **Supplementary Table 1**). A subset of lines with different sensitivity and genetic background was selected to better characterize the *in vitro* response. As indicated by the activation of caspase 3/7,

pevonedistat selectively induced apoptotic cell death in sensitive cells, regardless of the presence of mutations in *BRAF* or *KRAS* (**Figure 1B**). All responsive cells also displayed a dramatic increase in the fraction of cells with DNA content > 4N (**Figure 1C**), indicative of profound cell cycle alterations leading to re-replication, a known effect of NEDD8 pathway inhibition (21). To date, only one CRC cell line (HCT-116) has been tested for response to pevonedistat *in vivo*, in mouse xenografts (20). To further evaluate the *in vivo* activity of this compound on CRC models, the most sensitive cell line in the panel (HuTu-80) was xenotransplanted in nude mice, which were then treated with pevonedistat. As shown in **Supplementary Figure 1**, drug treatment induced tumor stabilization, similarly to what had previously been reported in HCT116 xenografts (20). Immunohistochemistry (IHC) on HuTu-80 explanted tumors highlighted pevonedistat-induced reduction of proliferating cells and accumulation of the known CRL substrate p21 (**Supplementary Figure 1**), indicating *in vivo* drug target engagement.

Molecular correlates of response to pevonedistat in CRC cell lines

Cell lines stratified by the following molecular features were assessed for differential pevonedistat sensitivity in vitro (**Figure 2A**): (i) MSI status; (ii) BRAF or *RAS* mutation; (iii) cetuximab sensitivity in *KRAS*/*BRAF* wild type cells; (iv) assignment to one of the three major transcriptional subtypes: Inflammatory/Goblet, TA/Enterocyte and Stem/Serrated/Mesenchymal, as summarized in **Supplementary Table 1** (35). While MSI status, *BRAF* or *RAS* mutations, and cetuximab sensitivity did not exhibit a statistically significant association with pevonedistat sensitivity or resistance, the TA/enterocyte transcriptional subtype, known to be enriched in cetuximab-sensitive cells (9), displayed statistically significant pevonedistat resistance *(t* test, viability in TA/enterocyte cell lines vs all other cell lines, P = .005;) Indeed, out of the 47 cell lines assigned to the TA/enterocyte subtype, only one displayed borderline sensitivity to pevonedistat.

We then exploited gene expression profiles to assess whether pevonedistat sensitivity was associated to specific transcriptional traits. To this aim, genes were ranked for differential expression between the 16 most sensitive and the 44 most resistant lines (**Figure 2B**; **Supplementary Table 1**) and tested for preferential up- or down-regulation of gene functional signatures, according to the Gene Set Enrichment Analysis (36) (GSEA; **Figure 2C**). GSEA highlighted upregulation of epithelial mesenchymal transition (EMT), hypoxia and TNF-alpha/NFKB pathways in pevonedistat-sensitive models. Interestingly, transcriptional signatures of EGFR/KRAS pathway activation and signaling dependence were instead upregulated in the pevonedistat-resistant group, in line with the above-described lower response to pevonedistat of TA/enterocyte subtype cells. Overall, this analysis confirmed that sensitivity to pevonedistat is associated with specific biological features, which are captured by transcriptional profiles.

A transcriptional predictor of pevonedistat sensitivity was thus built by selecting the genes with statistically significant differential expression between the most sensitive and most resistant cell lines, which resulted in 184 gene transcripts distinguishing sensitive from resistant cells (**Figure 2D**; **Supplementary Table 2**). A "pevonedistat sensitivity score" (PSS) was calculated for each cell line by subtracting the averaged expression values of genes upregulated in resistant cells from the average expression of genes upregulated in sensitive cells (**Supplementary Table 3**). To verify the robustness of this approach, we performed a full leave-one-out (LOO) cross-validation, so that each sample received a LOO-PSS from a signature built in a training dataset from which it was removed. The performance of PSS and LOO PSS were evaluated by ROC curves, resulting in AUC values of 0.96 and 0.91, respectively ($P < .001$ for both) (**Supplementary Figure 2**).

Preclinical validation of the pevonedistat response transcriptional predictor

To provide independent, preclinical *in vivo* validation of pevonedistat activity and of its transcriptional predictor in CRC, we applied the 184-gene predictor to an expression dataset generated from 87 LM-CRC samples, for which PDX derivatives were available. Of the 184 genes identified in cell lines, 163 were also detected in the LM-CRC dataset. This enabled derivation of a PSS whereby PDX samples were ranked by predicted sensitivity (**Figure 3A**; **Supplementary Table 3**). For validation purposes, six PDX models, were selected from samples with high PSS and five from samples with low PSS (**Supplementary Table 3**). In the final cohort, KRAS mutants, BRAF mutants and wild-type cases were represented in both groups, with the notable exception that no BRAF-mutant case had a low score.

For each model, at least six xenografts were treated with pevonedistat - and a corresponding cohort with vehicle - for 4 weeks. As shown in **Figure 3B**, no low-PSS model displayed statistically significant growth inhibition. Conversely, five out of the six models with high score were growth-inhibited by 80% or more ($P < .01$). In four cases, growth curve analysis (**Figure 3C**; **Supplementary Figure 3**) showed prolonged tumor stabilization by pevonedistat. As observed in cell line xenografts, highly sensitive PDXs displayed pevonedistat-induced Ki67 downregulation ($P < .001$) and accumulation of the CRLs substrates p21 ($P < .001$) and p27 ($P < .001$), detected by IHC (**Figure 4**) and confirmed by western blot analysis (**Supplementary Figure 4**). Altogether, these results confirm that an appreciable fraction of CRCs responds to NEDD8 pathway inhibition by pevonedistat *in vivo*. Importantly, the transcriptional predictor of response generated in cell lines efficiently identified responsive LM-CRC cases, which included also KRAS or BRAF mutant tumors.

Association of pevonedistat response prediction with clinical aggressiveness and poor differentiation of CRC.

To assess whether CRC cases predicted to respond to pevonedistat might have distinctive clinical features, the 184-gene predictor was applied to gene expression profiles from 290 CRC samples annotated for disease-free survival (DFS) after surgery (32) (GEO ID: GSE14333; **Supplementary Table 3**). As shown in **Figure 5A**, cases predicted to be sensitive to pevonedistat (top 15% highest PSS) had statistically significantly lower DFS (log rank chi square, P = .003, HR = 2.49, 95% CI = 1.34 to 4.62). ROC Curve analysis in this dataset highlighted that PSS has a statistically significant correlation with poor prognosis when used as a continuous variable (**Supplementary Figure 5A-B**). The predictor was then applied to LM-CRC samples annotated for clinical response to cetuximab (33) (GEO ID: GSE5851; **Supplementary Table 3**). In agreement with the results obtained *in vitro*, predicted sensitivity to pevonedistat was associated to statistically significantly lower progression-free survival (PFS) in patients treated with cetuximab monotherapy (log rank chi square , P < .001, HR = 3.59, 95% CI = 1.60 to 8.04; **Figure 5B**). Together with KRAS, the only negative predictor of Cetuximab efficacy available in this dataset, PSS displayed also statistically significant association with shorter PFS in univariate Cox regression analysis (PSS: HR = 2.44, 95% CI = 1.35 to 4.41, P = .003; KRAS: HR = 1.44, 95% CI = 1.0 to 2.05, P = .05), while in multivariate analysis, they both lost statistical significance (PSS: HR = 1.90, 95% CI = 0.95 to 3.79, P = .07; KRAS: HR = 1.37, 95% CI = 0.96 to 1.95, P = .09; data not shown).

We then evaluated possible relationships between the pevonedistat sensitivity signature and established morphological markers currently in use for CRC stratification. We noticed that many known markers of CRC differentiation were downregulated in sensitive cell lines (**Supplementary Figure 5C-F**), suggesting that a positive prediction of response could be associated with poor differentiation. To verify this hypothesis, a transcriptional colon tissue-specific score that we previously calculated for all CRC cell lines (9) was compared with the PSS, and found to be inversely correlated (**Figure 5C**; Pearson r = -0.88, correlation significance test: P < .001, 95% CI = 0.83 to

0.91). Indeed, most of the colon differentiation genes were massively downmodulated in pevonedistat-sensitive lines, as shown by GSEA analysis (**Figure 5D**). Accordingly, pevonedistat-sensitive cell lines had a statistically significantly lower colon score than pevonedistat-resistant cells (**Figure 5E**; *t* test, colon score in pevonedistat-sensitive cells vs. all others, P < .001; correlation between colon score and cell viability upon pevonedistat treatment, Pearson r = 0.40, correlation significance test: P < .001, 95% CI = 0.24 to 0.54). Conversely, cetuximab-sensitive models were characterized by a statistically significantly higher colon score (**Figure 5F**; *t* test, colon score in cetuximab-sensitive cells vs all others P < .001; correlation between colon score and cell viability upon cetuximab treatment, Pearson *r* = -0.38, correlation significance test: P < .001, 95% CI = -0.22 to -0.52). Interestingly, the colon tissue-specific score was statistically significantly lower in BRAF-mutated cells and in the SSM subtype, while it was statistically significantly higher in the TA/enterocyte subtype (**Supplementary Figure 6**). These results are in agreement with the less statistically significant trends observed with the pevonedistat response in **Figure 2A**. Overall, these results indicate that pevonedistat sensitivity and its transcriptional predictor are associated with poor differentiation in CRC cell lines.

Of the four known CRC differentiation markers with the highest differential value between pevonedistat-sensitive and resistant cells (*CDH17*, *KRT20*, *CDX1* and *CDX2*), *cadherin-17* mRNA proved to be the most inversely correlated with the PSS in the 87 liver metastases dataset (Pearson correlation = -0.68, correlation significance test: P < .001, 95% CI = -0.78 to -0.55 (data not shown) . We therefore selected a representative set of 15 CRC liver metastasis samples with variable PSS and stained them for *CDH17* protein expression by IHC. Protein levels of *CDH17* were well correlated with the respective mRNA levels (**Supplementary Figure 7**) and, most importantly, displayed a strong inverse correlation with the PSS (**Figure 5G**; Pearson *r* = -0.74, 95% CI = -0.91 to -0.37, P = .002). *CDH17* protein expression was also evaluated in the 11 PDX models selected for *in vivo* tests, and again found to be inversely correlated with response to pevonedistat expressed as growth inhibition

(Pearson r = -0.77, 95% CI = -0.94 to -0.32, P = .006; **Figure 5H**). As a further validation, two pathologists scored CDH17 levels independently in 22 CRC tissues from PDXs. The results, displaying good concordance (kappa = 0.771), were highly correlated with CDH17 RNA levels measured by qPCR (**Supplementary Figure 7C**) on the same samples (Pearson correlation r = 0.79; correlation significance test: P < .001, 95% CI: 0.55 to 0.91). These data confirm *CDH17* protein or mRNA detection as a potentially valuable negative predictor of pevonedistat sensitivity in CRC.

To evaluate possible positive morphological predictors of pevonedistat sensitivity, hematoxylin/eosin-stained sections of CRC liver metastases with variable PSS values were independently analyzed by two pathologists. Interestingly, all mucinous adenocarcinoma samples invariably had high PSS values, while the great majority of non-mucinous and mixed cases had low or negative PSS (**Figure 6A**). The mucinous histotype was strongly associated with low *CDH17* expression (**Figure 6B**). Univariate and multivariate linear regression analyses in the 87 CRC-LM dataset did not highlight association of CHD17 expression with MSI status, KRAS or other mutation, and cetuximab sensitivity, while association with PSS remained independently statistically significant. The same pattern was observed in the 11 PDX models selected for *in vivo* tests, where the mucinous histotype was invariably detected in all pevonedistat-responsive cases, but not in the five resistant cases with low PSS (**Figure 6C-D**; **Supplementary Figure 8A-C**). The only case with mucinous histotype and high PSS that did not respond to pevonedistat, M024, displayed instead high CDH17 expression (**Supplementary Figure 8D**).

Discussion

In this work, we exploited a large tissue-specific collection of CRC cell lines to assess pevonedistat efficacy; we defined in this cohort a transcriptional predictor of response; and, finally, we applied the predictor to a powerful preclinical platform, composed of fresh tumor samples matched with PDX

derivatives, that reliably mirror disease response and its correlation with predictive biomarkers (9, 27). The 122 CRC cell lines selected for pevonedistat testing covered the whole spectrum of CRC molecular and transcriptional subtypes known to date (9). The fraction of responsive cell lines was even higher than that of cetuximab-sensitive models. The main biological responses elicited by pevonedistat in sensitive CRC lines were re-replication, G2 arrest and apoptosis, in agreement with previous findings in solid tumors and hematological malignancies (20, 21). Of relevance, the observed functional inverse correlation with EGFR pathway activity/dependence and the lack of statistically significant association with *KRAS* or *BRAF* mutation render this therapeutic approach potentially eligible also for cetuximab-resistant and 'RAS' pathway-mutant CRC.

Gene expression profiling of CRC cell lines at the baseline provided further information about functional features associated with pevonedistat sensitivity/resistance. In particular, pevonedistat-sensitive cells displayed transcriptional traits of EMT, possibly driven by hypoxia and TNFα signaling (37-39), a phenotype associated to poor prognosis of CRC (40, 41). Conversely, resistant cell lines displayed marked traits of EGFR/KRAS pathway activity and associated sensitivity to EGFR blockade (42, 43). These results confirmed that global transcriptome analysis could reliably capture functional traits associated with pevonedistat sensitivity or resistance. Indeed, the genes of the pevonedistat sensitivity signature, obtained by supervised analysis, displayed highly concordant expression across cell lines, indicative of coherent transcriptional modules. This signature was therefore applied as a response predictor in an independent dataset of 87 LM-CRCs. Although identified in *in vitro* cultured CRC cell lines, genes of the predictor displayed coherent expression also in LM-CRC samples, which allowed their stratification by a +/- 2.5-fold range of PSS. PDXs derived from high-PSS selected LM-CRCs were markedly sensitive to pevonedistat in five out of six cases, while none of the predicted resistant PDXs responded to pevonedistat treatment. This indicates that the transcriptional signature

can efficiently predict *in vivo* sensitivity. Notably, in all xenografts tested, pevonedistat did not display detectable side effects.

Tumor response achieved in sensitive PDX models was growth stabilization, rather than regression. Of note, and in line with the tumor stabilization observed in phase I clinical trials (25), these results do not reflect the extensive cell death and profound growth inhibition observed for sensitive cell lines *in vitro*. The same discrepancy was seen when xenografts from the most sensitive of the 122 cell lines were treated with pevonedistat, which only induced tumor stabilization (Supplementary Figure 1). This suggests that the lack of tumor regression *in vivo* could be due to suboptimal drug delivery/pharmacodynamics and/or microenvironmental protective factors. However, given the uniqueness of the pathway affected, it is likely pevonedistat will have additive or synergistic effects when combined with other treatments. Indeed, preclinical evidence of improved efficacy by combination with pevonedistat has already been obtained for apoptosis inducers like TRAIL and TNF-α (44, 45), DNA-damaging agents (46-50) and radiation therapy (18, 51). Some of these combinations are currently being evaluated in clinical trials on unselected cases (NCT01862328). Future exploration of similar combinations in CRC will greatly benefit from the possibility of selecting patients by the predictor described here.

From the clinical point of view, it should be noted that the gene expression-based predictor of pevonedistat response captured a subset of cases with distinctive prognostic, pharmacological and morphofunctional features: (i) human CRC samples with high PSS had a statistically significantly worse prognosis; (ii) observed or predicted pevonedistat sensitivity was inversely associated to cetuximab sensitivity, from cell lines to patients, and occurred also in *KRAS*- and *BRAF*-mutant cases, intrinsically resistant to EGFR blockade; (iii) low mRNA and protein levels of the differentiation marker CDH17 (52), encoding for a cell-adhesion molecule expressed in intestinal epithelium, were strongly correlated to pevonedistat sensitivity in vitro and *in vivo*. Therefore, positive CDH17 IHC

staining could be exploited as a negative predictor of pevonedistat response; conversely, a positive predictor could be the high grade, mucinous phenotype, which accounts for about 10% of CRCs and is characterized by adverse prognosis and poor response to chemotherapy and targeted agents (53-55). Recently, low-grade mucinous CRCs have been distinguished from high-grade cases by their differentiated morphology (56). Notably, all the five PDX models displaying sensitivity to pevonedistat were poorly differentiated (CDH17-negative) and mucinous, therefore belonging to the high-grade mucinous subgroup.

The main limitation of the results presented here is that pevonedistat efficacy has only been evaluated preclinically, in cell lines and PDXs. Also, the activity of pevonedistat in combination with current therapeutic regimens for CRC has not been explored. Treatment efficacy, alone or in combination, and its associated predictors deserve prospective clinical validation on CRC patients.

In summary, this study shows that NEDD8 pathway inhibition by pevonedistat may be a promising therapeutic strategy for poorly differentiated mucinous CRC. Response to pevonedistat of this clinically aggressive histotype of CRC occurs also in the presence of KRAS or BRAF activating mutations, that typically compromise the efficacy of commonly used targeted treatments focused on the EGFR pathway.

Funding

This work was supported by Associazione Italiana per la Ricerca sul Cancro (AIRC) investigator grants (IG12944 to E. Medico, IG17707 to F. Di Nicolantonio; IG14205 to L. Trusolino, IG15571 to A. Bertotti and IG 12812 to A. Bardelli), Associazione Italiana per la Ricerca sul Cancro (AIRC) 9970-2010 Special Program Molecular Clinical Oncology 5x1000 to E. Medico, L. Trusolino and A.

Bardelli; Fondazione Piemontese per la Ricerca sul Cancro 5x1000 Ministero della Salute 2010 and 2011 to E. Medico, L. Trusolino and A. Bardelli; American Association for Cancer Research – Fight Colorectal Cancer Career Development Award in memory of Lisa Dubow (12-20-16-BERT) to A. Bertotti; European Community's Seventh Framework Programme under grant agreement no. 602901 MErCuRIC (A. Bardelli); IMI contract n. 115749 CANCER-ID (A. Bardelli); Ministero dell'Istruzione, dell'Università e della Ricerca - progetto PRIN 2010-2011 (A. Bardelli).

Note

The funders had no role in design of the study; the collection, analysis, or interpretation of the data; the writing of the manuscript; or the decision to submit the manuscript for publication.

Acknowledgments: We thank Carlotta Cancelliere, Roberta Porporato, Barbara Martinoglio, Daniela Cantarella, Erica Torchiaro and Sara Erica Bellomo for technical assistance, and Simona Destefanis for secretarial assistance. E.M., A.B. and L.T. are members of the EurOPDX Consortium.

Author contributions: G.Picco contributed study design, data analysis, performed *in vitro* and *in vivo* experiments and manuscript writing. C. Petti performed *in vivo* and *in vitro* experiments. K. Grillone and T. Rossi performed *in vitro* experiments. G. Migliardi contributed to *in vivo* experiments. C. Isella contributed to bioinformatics analyses. F. Sassi, I. Sarotto and A. Sapino performed and interpreted histochemical and morphological analyses. L.Trusolino, A. Bardelli, F. Di Nicolantonio and A. Bertotti contributed study design and manuscript writing. E. Medico contributed study design, data analysis, bioinformatics, manuscript writing and project oversight.

Competing interests: The authors declare no competing financial interests.

Figure legends

Figure 1. Sensitivity of CRC cell lines to Pevonedistat in vitro. (**A**) The indicated cell lines (n=122) were treated with increasing concentrations of Pevonedistat for 4 days and cell viability was assessed by measuring ATP content. Bars represent relative cell viability compared to vehicle after 96 hours of treatment (average between viability at 0.5 and viability at 1 μM pevonedistat). Cells lines with viability < 40% were considered sensitive (n=16; 13%). Red (sensitive) and blue (resistant) squares at the bottom of the bars highlight representative cell lines selected for further characterization of the response. (**B**) Histograms representing the relative caspase 3-7 activity of pevonedistat-sensitive (red) and resistant (blue) cell lines after 48h of exposure to the drug at incremental concentration, as indicated. Caspase activity was normalized versus viability values (CellTiter-Glo), obtained from experiments performed in parallel ± SD (n = 3). (**C**) DNA content evaluation by flow cytometry in CRC cell lines. Black histograms: vehicle-treated cells. Colored histograms: cells treated for 24h with 1μM pevonedistat. Only sensitive cell lines display a remarkable increase of re-replicating cells (>4n) when treated with pevonedistat (red histograms). The dotted vertical line indicates the threshold for DNA content >4n. The fraction of re-replicating cells in vehicle- and pevonedistat-treated cells is reported in black and colored boxes, respectively.

Figure 2. Molecular prediction of pevonedistat sensitivity in CRC cell lines. (**A**) Dot plots displaying sensitivity to Pevonedistat (average viability at 0.5 and 1 μM) of 122 CRC cell lines stratified by MSI status, KRAS/BRAF mutational status, cetuximab sensitivity (only in KRAS and BRAF wild-type cases) and consensus transcriptional subtypes, as indicated. (**B**) Dose-response to Pevonedistat of 16 highly sensitive and 44 highly resistant CRC cell lines (red and blue curves, respectively). (**C**) Outcome of GSEA analysis displaying the most statistically significant gene sets upregulated (red text) or downregulated (blue text) in pevonedistat-sensitive CRC cell lines. The radar

plot scale indicates the GSEA normalized enrichment score (NES). (**D**) Heatmap representing the expression of the 184 signature genes (rows) in pevonedistat-sensitive and resistant cell lines, ordered from left to right by decreasing sensitivity score.

Figure 3. *In vivo* response to pevonedistat of CRC PDXs with high or low predicted sensitivity. (**A**) Waterfall plot displaying 87 CRC liver metastases ordered by decreasing pevonedistat sensitivity score (PSS, y-axis), from left to right. Red and blue bars highlight cases with high and low PSS, selected for validation in PDX models. The heatmap reports expression (log2 ratio vs average) of signature genes in the same 87 samples. (**B**) Bar graph reporting growth inhibition of PDXs after treatment for 28 days with Pevonedistat vs vehicle-treated counterparts. Red bars, high PSS cases; blue bars, low PSS cases. Sample ID, KRAS/BRAF mutational status and PSS is reported at the bottom of each bar. Asterisks on top of the bars indicate statistically significant growth inhibition after 28 days of treatment (Student's t-test, **P < .01; ***P < .001) (**C**) PDX growth curves (median ± SD) of the cases displaying the highest growth inhibition among the predicted sensitive (left panels, red curves) and among the predicted resistant (right panels, blue curves). Black curves, vehicle-treated.

Figure 4. In vivo changes of ki67, p21 and p27 protein levels upon pevonedistat treatment of CRC PDXs. Immunohistochemical staining and morphometric quantitation of ki67 (**A**), p21 (**B**) and p27 (**C**) of two representative PDX tumors derived from a sensitive (M085, red bars) and a resistant (M065, blue bars) case at the end of treatment with vehicle (black bar) or pevonedistat (colored bar), as indicated. Results are means ± SD of 10 fields (20×) for each experimental point. Bar graphs are flanked by micrographs of representative fields. Scale bar, 50 μm.

Figure 5. Association between predicted pevonedistat sensitivity, clinical aggressiveness and poor differentiation of CRC. (**A**) Kaplan-Meier analysis of disease-free survival after surgery of primary CRC cases with top 15% highest PSS score (red line) vs all remaining cases (blue line). (**B**) Kaplan-Meier analysis of progression-free survival of liver metastatic cases with top 15% highest PSS score (red line) after treatment with cetuximab monotherapy. (**C**) Dot plot displaying the correlation between the PSS (y-axis) and the tissue-specific "colon" score (x-axis) in 122 CRC cell lines. (**D**) GSEA enrichment analysis of colon differentiation genes in pevonedistat-sensitive vs resistant cell lines. Dot plots displaying the correlation between the tissue-specific "colon" score and viability upon pevonedistat (**E**) and cetuximab (**F**) treatment. Pevonedistat-sensitive lines are marked in red (left panel), cetuximab sensitive lines are marked in blue (right panel). (**G**) Correlation between PSS and CDH17 protein expression detected by IHC in 16 liver metastatic CRC samples. (**H**) Correlation between growth inhibition measured in 11 PDXs tested in vivo and CDH17 protein expression of the same PDXs evaluated by IHC. All statistical tests were two-sided. P values are from: panels A-B, log rank chi square test; panels E-H, the SISA online calculator for statistical significance of a correlation (www.quantitativeskills.com/sisa/statistics/correl.htm).

Figure 6. Association of Pevonedistat sensitivity with the high-grade mucinous CRC histotype. (**A**) Dot plot reporting on the x-axis the PSS values for CRC liver metastases grouped by their mucinous aspect: mucinous, mixed, non-mucinous. (**B**) Bar plot showing, on the y-axis, the fraction of mucinous (red), mixed (grey) and non-mucinous (blue) cases grouped by their CDH17 staining signal, from 1 (absent) to 4 (high). (C-D) Micrographs of representative PDXs responsive or resistant to pevonedistat (left and right panels, respectively), stained by haematoxylin and eosin. Scale bar 50 μm.

References

1. Kamiyama H, Noda H, Konishi F, *et al.* Molecular biomarkers for the detection of metastatic colorectal cancer cells. World J Gastroenterol 2014;20(27):8928-38.
2. Chung KY, Shia J, Kemeny NE, *et al.* Cetuximab shows activity in colorectal cancer patients with tumors that do not express the epidermal growth factor receptor by immunohistochemistry. J Clin Oncol 2005;23(9):1803-10.
3. Cunningham D, Humblet Y, Siena S, *et al.* Cetuximab monotherapy and cetuximab plus irinotecan in irinotecan-refractory metastatic colorectal cancer. N Engl J Med 2004;351(4):337-45.
4. Misale S, Di Nicolantonio F, Sartore-Bianchi A, *et al.* Resistance to anti-EGFR therapy in colorectal cancer: from heterogeneity to convergent evolution. Cancer Discov 2014;4(11):1269-80.
5. De Roock W, Claes B, Bernasconi D, *et al.* Effects of KRAS, BRAF, NRAS, and PIK3CA mutations on the efficacy of cetuximab plus chemotherapy in chemotherapy-refractory metastatic colorectal cancer: a retrospective consortium analysis. Lancet Oncol 2010;11(8):753-62.
6. Misale S, Yaeger R, Hobor S, *et al.* Emergence of KRAS mutations and acquired resistance to anti-EGFR therapy in colorectal cancer. Nature 2012;486(7404):532-6.
7. Bertotti A, Papp E, Jones S, *et al.* The genomic landscape of response to EGFR blockade in colorectal cancer. Nature 2015;526(7572):263-7.
8. Bertotti A, Migliardi G, Galimi F, *et al.* A molecularly annotated platform of patient-derived xenografts ("xenopatients") identifies HER2 as an effective therapeutic target in cetuximab-resistant colorectal cancer. Cancer Discov 2011;1(6):508-23.
9. Medico E, Russo M, Picco G, *et al.* The molecular landscape of colorectal cancer cell lines unveils clinically actionable kinase targets. Nat Commun 2015;6:7002.
10. Kamitani T, Kito K, Nguyen HP, *et al.* Characterization of NEDD8, a developmentally down-regulated ubiquitin-like protein. J Biol Chem 1997;272(45):28557-62.
11. Rabut G, Peter M. Function and regulation of protein neddylation. 'Protein modifications: beyond the usual suspects' review series. EMBO Rep 2008;9(10):969-76.
12. Watson IR, Irwin MS, Ohh M. NEDD8 pathways in cancer, Sine Quibus Non. Cancer Cell 2011;19(2):168-76.
13. Sarikas A, Hartmann T, Pan ZQ. The cullin protein family. Genome Biol 2011;12(4):220.
14. Soucy TA, Smith PG, Rolfe M. Targeting NEDD8-activated cullin-RING ligases for the treatment of cancer. Clin Cancer Res 2009;15(12):3912-6.
15. Micel LN, Tentler JJ, Smith PG, *et al.* Role of ubiquitin ligases and the proteasome in oncogenesis: novel targets for anticancer therapies. J Clin Oncol 2013;31(9):1231-8.
16. Gu Y, Kaufman JL, Bernal L, *et al.* MLN4924, an NAE inhibitor, suppresses AKT and mTOR signaling via upregulation of REDD1 in human myeloma cells. Blood 2014;123(21):3269-76.
17. Wang X, Zhang W, Yan Z, *et al.* Radiosensitization by the investigational NEDD8-activating enzyme inhibitor MLN4924 (pevonedistat) in hormone-resistant prostate cancer cells. Oncotarget 2016; 10.18632/oncotarget.9526.
18. Yang D, Tan M, Wang G, *et al.* The p21-dependent radiosensitization of human breast cancer cells by MLN4924, an investigational inhibitor of NEDD8 activating enzyme. PLoS One 2012;7(3):e34079.
19. Li L, Wang M, Yu G, *et al.* Overactivated neddylation pathway as a therapeutic target in lung cancer. J Natl Cancer Inst 2014;106(6):dju083.
20. Soucy TA, Smith PG, Milhollen MA, *et al.* An inhibitor of NEDD8-activating enzyme as a new approach to treat cancer. Nature 2009;458(7239):732-6.
21. Lin JJ, Milhollen MA, Smith PG, *et al.* NEDD8-targeting drug MLN4924 elicits DNA rereplication by stabilizing Cdt1 in S phase, triggering checkpoint activation, apoptosis, and senescence in cancer cells. Cancer Res 2010;70(24):10310-20.
22. Jia L, Li H, Sun Y. Induction of p21-dependent senescence by an NAE inhibitor, MLN4924, as a mechanism of growth suppression. Neoplasia 2011;13(6):561-9.
23. Zhang Q, Hou D, Luo Z, *et al.* The novel protective role of P27 in MLN4924-treated gastric cancer cells. Cell Death Dis 2015;6:e1867.
24. Shah JJ, Jakubowiak AJ, O'Connor OA, *et al.* Phase I Study of the Novel Investigational NEDD8-Activating Enzyme Inhibitor Pevonedistat (MLN4924) in Patients with Relapsed/Refractory Multiple Myeloma or Lymphoma. Clin Cancer Res 2015; 10.1158/1078-0432.CCR-15-1237.
25. Sarantopoulos J, Shapiro GI, Cohen RB, *et al.* Phase I Study of the Investigational NEDD8-activating Enzyme Inhibitor Pevonedistat (TAK-924/MLN4924) in Patients with Advanced Solid Tumors. Clin Cancer Res 2015; 10.1158/1078-0432.CCR-15-1338.

26. Swords RT, Erba HP, DeAngelo DJ, *et al.* Pevonedistat (MLN4924), a First-in-Class NEDD8-activating enzyme inhibitor, in patients with acute myeloid leukaemia and myelodysplastic syndromes: a phase 1 study. Br J Haematol 2015;169(4):534-43.
27. Bertotti A, Migliardi G, Galimi F, *et al.* A molecularly annotated platform of patient-derived xenografts ("xenopatients") identifies HER2 as an effective therapeutic target in cetuximab-resistant colorectal cancer. Cancer Discov 2011;1(6):508-23.
28. Maletzki C, Stier S, Gruenert U, *et al.* Establishment, characterization and chemosensitivity of three mismatch repair deficient cell lines from sporadic and inherited colorectal carcinomas. PLoS One 2012;7(12):e52485.
29. Maletzki C, Huehns M, Knapp P, *et al.* Functional Characterization and Drug Response of Freshly Established Patient-Derived Tumor Models with CpG Island Methylator Phenotype. PLoS One 2015;10(11):e0143194.
30. Maletzki C, Gock M, Randow M, *et al.* Establishment and characterization of cell lines from chromosomal instable colorectal cancer. World J Gastroenterol 2015;21(1):164-76.
31. Fu L, Medico E. FLAME, a novel fuzzy clustering method for the analysis of DNA microarray data. BMC Bioinformatics 2007;8:3.
32. Jorissen RN, Gibbs P, Christie M, *et al.* Metastasis-Associated Gene Expression Changes Predict Poor Outcomes in Patients with Dukes Stage B and C Colorectal Cancer. Clin Cancer Res 2009;15(24):7642-7651.
33. Khambata-Ford S, Garrett CR, Meropol NJ, *et al.* Expression of epiregulin and amphiregulin and K-ras mutation status predict disease control in metastatic colorectal cancer patients treated with cetuximab. J Clin Oncol 2007;25(22):3230-7.
34. Gentleman RC, Carey VJ, Bates DM, *et al.* Bioconductor: open software development for computational biology and bioinformatics. Genome Biol 2004;5(10):R80.
35. Isella C, Terrasi A, Bellomo SE, *et al.* Stromal contribution to the colorectal cancer transcriptome. Nat Genet 2015;47(4):312-9.
36. Subramanian A, Tamayo P, Mootha VK, *et al.* Gene set enrichment analysis: a knowledge-based approach for interpreting genome-wide expression profiles. Proc Natl Acad Sci U S A 2005;102(43):15545-50.
37. Yang MH, Wu MZ, Chiou SH, *et al.* Direct regulation of TWIST by HIF-1alpha promotes metastasis. Nat Cell Biol 2008;10(3):295-305.
38. Hill RP, Marie-Egyptienne DT, Hedley DW. Cancer stem cells, hypoxia and metastasis. Semin Radiat Oncol 2009;19(2):106-11.
39. Li CW, Xia W, Huo L, *et al.* Epithelial-mesenchymal transition induced by TNF-Ã Â± requires NF-Ã ÂºB-mediated transcriptional upregulation of Twist1. Cancer Res 2012;72(5):1290-300.
40. Loboda A, Nebozhyn MV, Watters JW, *et al.* EMT is the dominant program in human colon cancer. BMC Med Genomics 2011;4:9.
41. Shelygin YA, Pospekhova NI, Shubin VP, *et al.* Epithelial-mesenchymal transition and somatic alteration in colorectal cancer with and without peritoneal carcinomatosis. Biomed Res Int 2014;2014:629496.
42. Fraguas S, BarberÃ Â¡n S, CebriÃ Â F. EGFR signaling regulates cell proliferation, differentiation and morphogenesis during planarian regeneration and homeostasis. Dev Biol 2011;354(1):87-101.
43. Amann J, Kalyankrishna S, Massion PP, *et al.* Aberrant epidermal growth factor receptor signaling and enhanced sensitivity to EGFR inhibitors in lung cancer. Cancer Res 2005;65(1):226-35.
44. Zhao L, Yue P, Lonial S, *et al.* The NEDD8-activating enzyme inhibitor, MLN4924, cooperates with TRAIL to augment apoptosis through facilitating c-FLIP degradation in head and neck cancer cells. Mol Cancer Ther 2011;10(12):2415-25.
45. F S Wolenski CDF, T Sano, S D Wyllie, L A Cicia, M J Gallacher, R A Baker, P J Kirby & J J Senn. The NAE inhibitor pevonedistat (MLN4924) synergizes with TNF-Ã Â±Ã Â to activate apoptosis. In; 2015.
46. Ho IL, Kuo KL, Liu SH, *et al.* MLN4924 Synergistically Enhances Cisplatin-induced Cytotoxicity via JNK and Bcl-xL Pathways in Human Urothelial Carcinoma. Sci Rep 2015;5:16948.
47. Nawrocki ST, Kelly KR, Smith PG, *et al.* The NEDD8-activating enzyme inhibitor MLN4924 disrupts nucleotide metabolism and augments the efficacy of cytarabine. Clin Cancer Res 2015;21(2):439-47.
48. Paiva C, Godbersen JC, Berger A, *et al.* Targeting neddylation induces DNA damage and checkpoint activation and sensitizes chronic lymphocytic leukemia B cells to alkylating agents. Cell Death Dis 2015;6:e1807.
49. Garcia K, Blank JL, Bouck DC, *et al.* Nedd8-activating enzyme inhibitor MLN4924 provides synergy with mitomycin C through interactions with ATR, BRCA1/BRCA2, and chromatin dynamics pathways. Mol Cancer Ther 2014;13(6):1625-35.
50. Jazaeri AA, Shibata E, Park J, *et al.* Overcoming platinum resistance in preclinical models of ovarian cancer using the neddylation inhibitor MLN4924. Mol Cancer Ther 2013;12(10):1958-67.
51. Wei D, Li H, Yu J, *et al.* Radiosensitization of human pancreatic cancer cells by MLN4924, an investigational NEDD8-activating enzyme inhibitor. Cancer Res 2012;72(1):282-93.

52. Panarelli NC, Yantiss RK, Yeh MM, *et al.* Tissue-specific cadherin CDH17 is a useful marker of gastrointestinal adenocarcinomas with higher sensitivity than CDX2. Am J Clin Pathol 2012;138(2):211-22.
53. Lee DW, Han SW, Lee HJ, *et al.* Prognostic implication of mucinous histology in colorectal cancer patients treated with adjuvant FOLFOX chemotherapy. Br J Cancer 2013;108(10):1978-84.
54. Numata M, Shiozawa M, Watanabe T, *et al.* The clinicopathological features of colorectal mucinous adenocarcinoma and a therapeutic strategy for the disease. World J Surg Oncol 2012;10:109.
55. Mekenkamp LJ, Heesterbeek KJ, Koopman M, *et al.* Mucinous adenocarcinomas: poor prognosis in metastatic colorectal cancer. Eur J Cancer 2012;48(4):501-9.
56. Yoshioka Y, Togashi Y, Chikugo T, *et al.* Clinicopathological and genetic differences between low-grade and high-grade colorectal mucinous adenocarcinomas. Cancer 2015;121(24):4359-68.

A

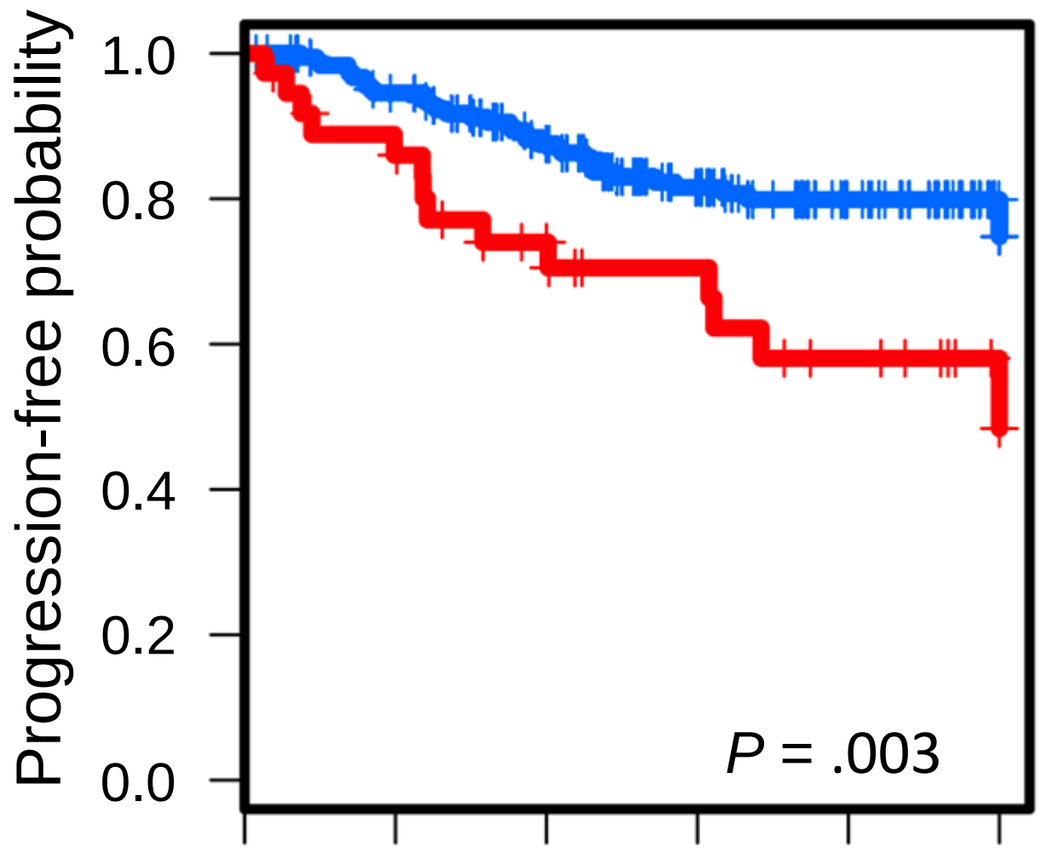

Years	0	1	2	3	4	5
	189	171	142	108	77	47
	37	30	22	17	12	6

B

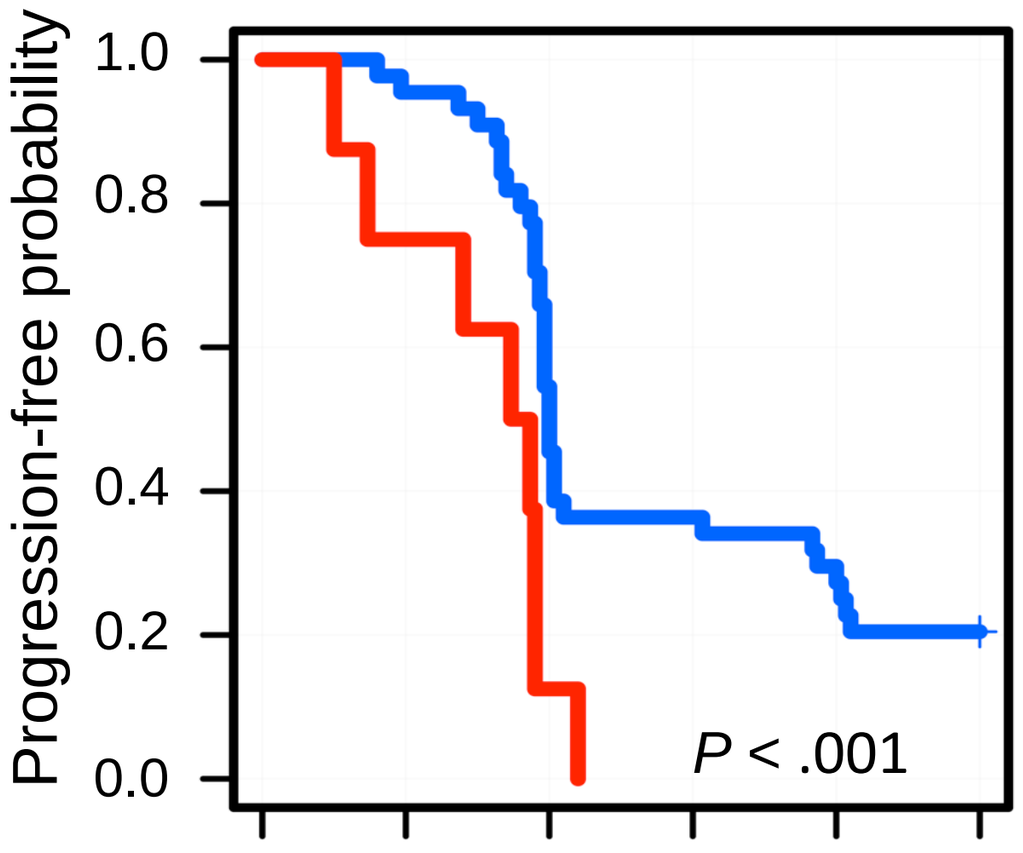

Days	0	30	60	90	120	150
	44	42	24	16	13	9
	8	6	1			

C

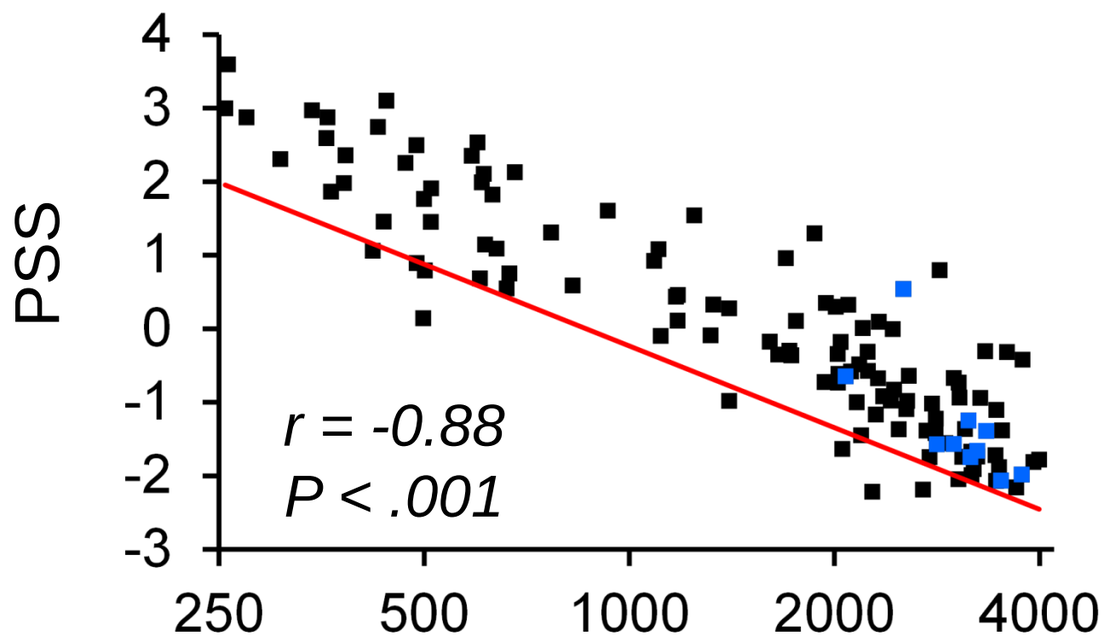

D

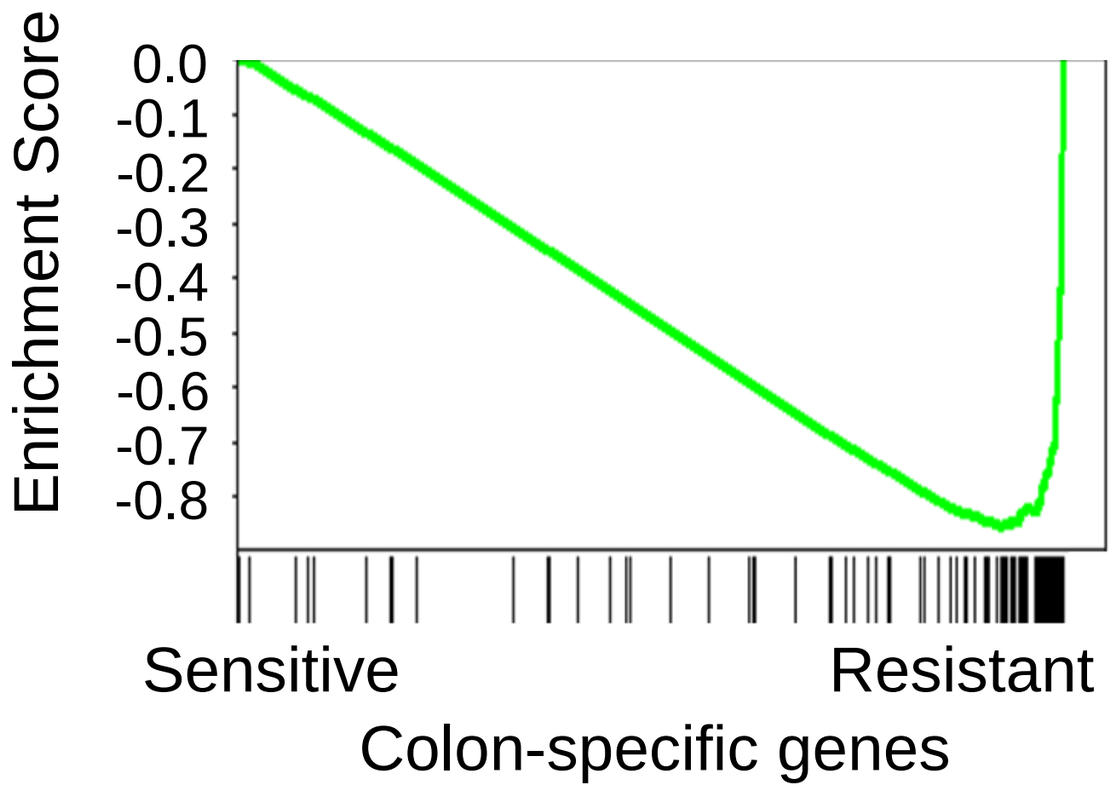

E

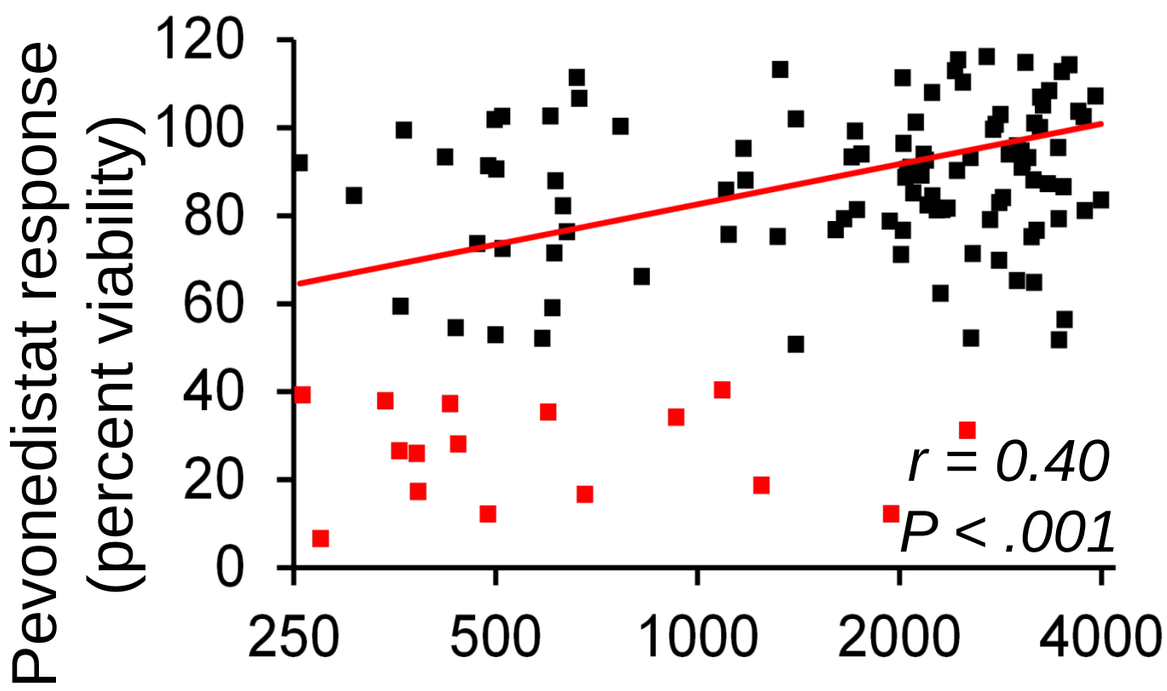

F

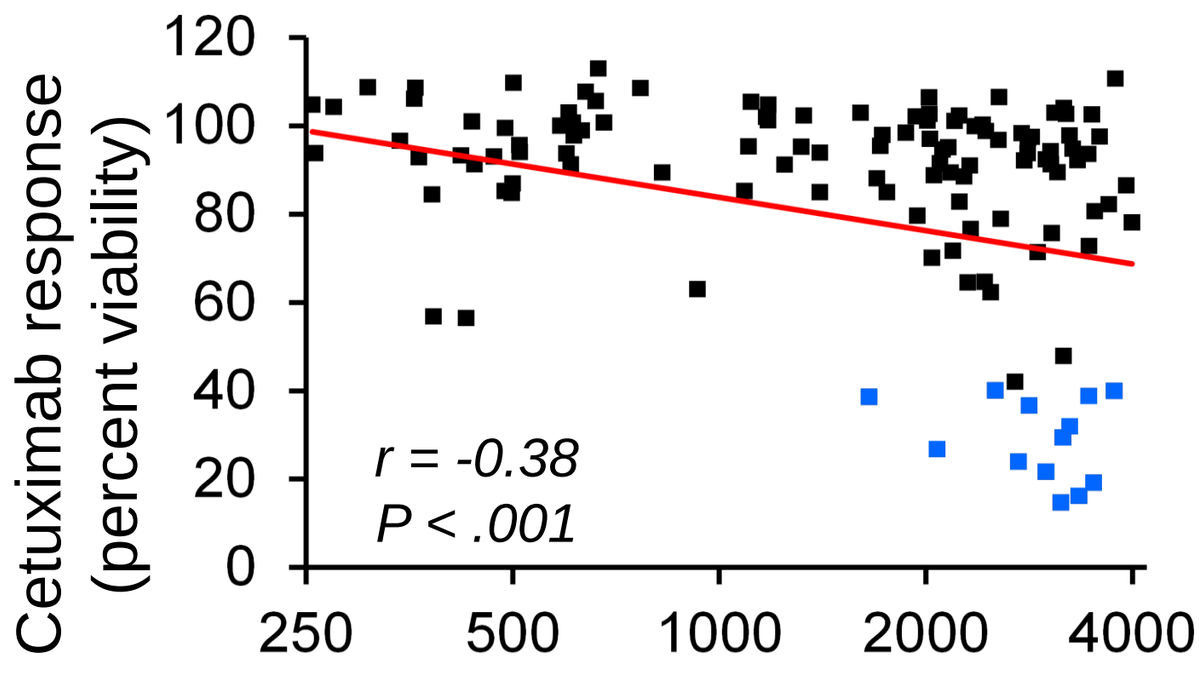

G

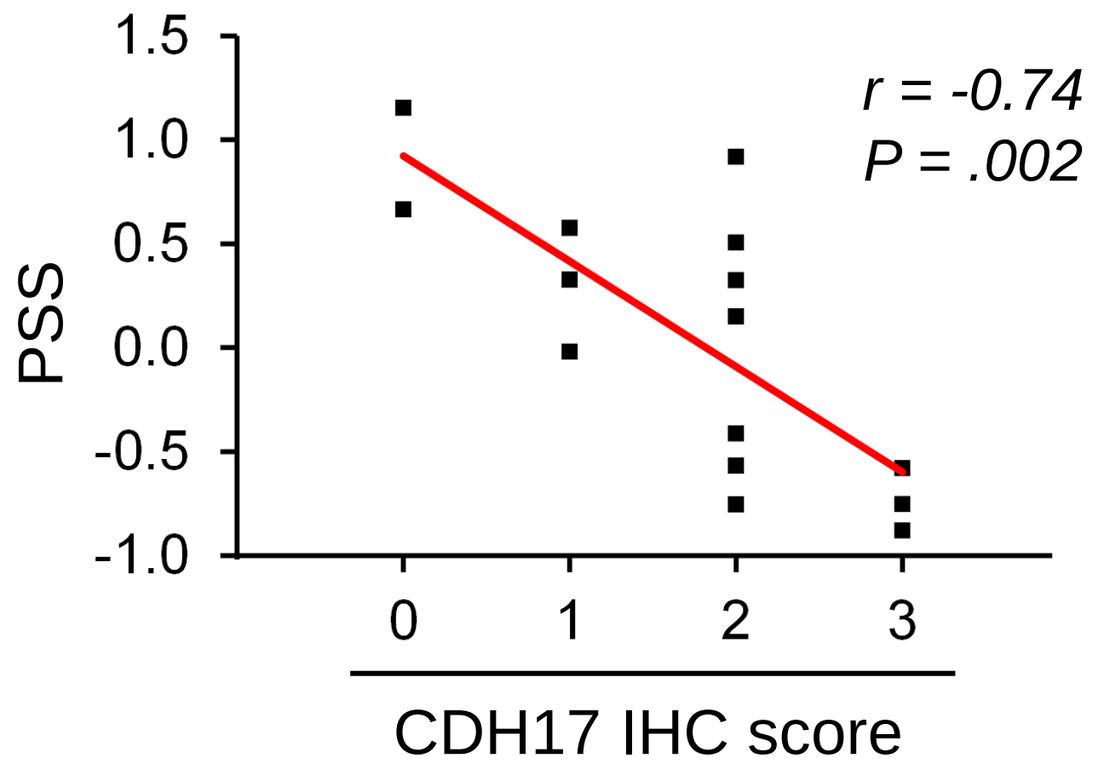

H

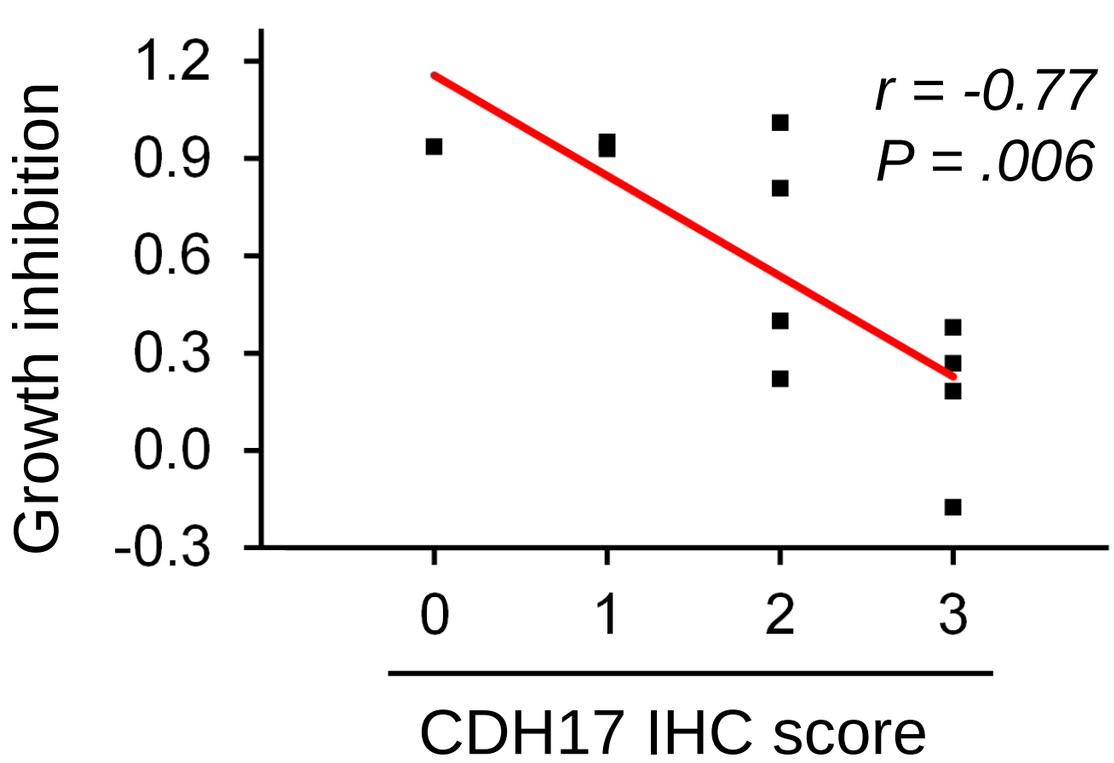

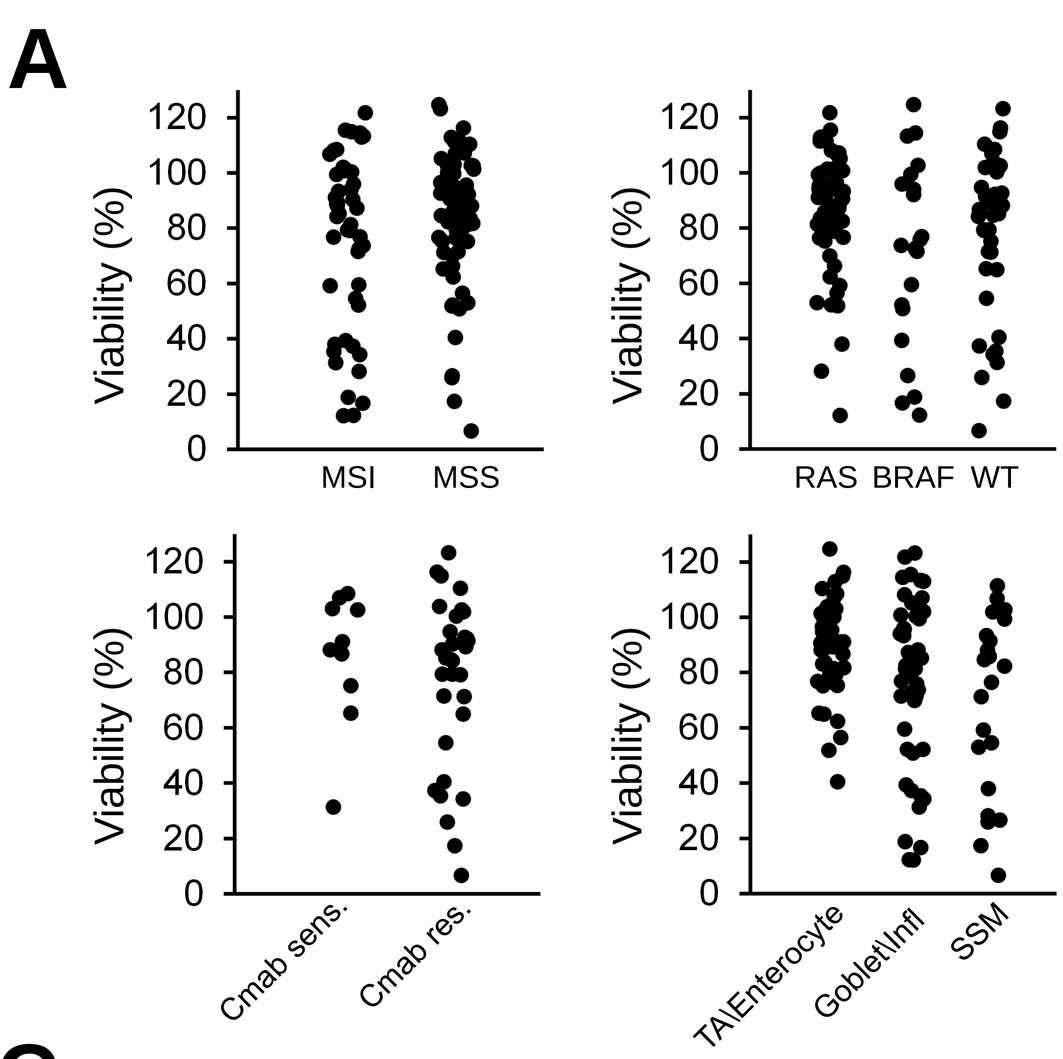
A
Viability (%)
120
100
80
60
40
20
0
MSI
MSS
RAS
BRAF
WT
Cmab sens.
Cmab res.
TA\Enterocyte
Goblet\Infl
SSM

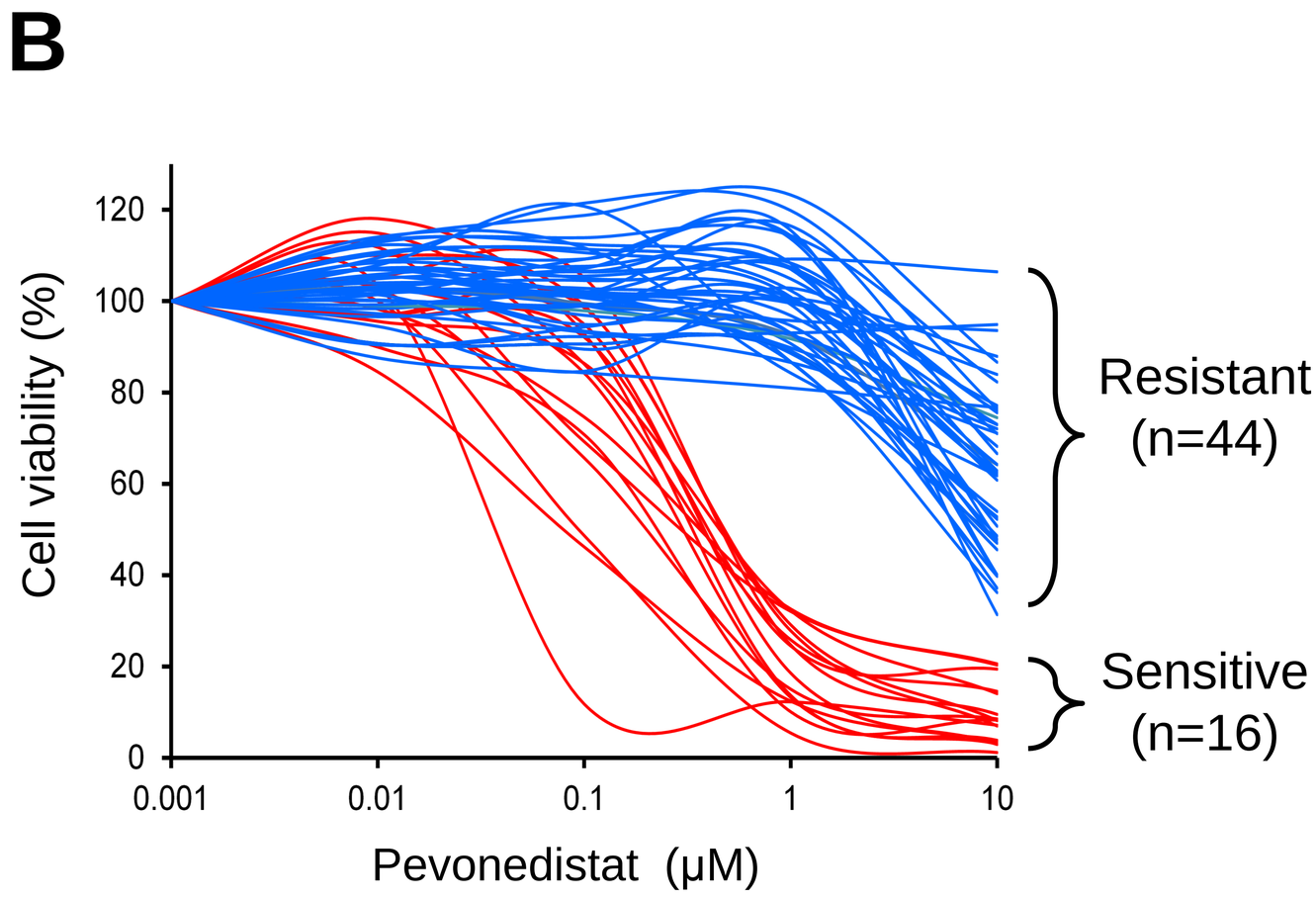
B
Cell viability (%)
120
100
80
60
40
20
0
0.001
0.01
0.1
1
10
Pevonedistat (μM)
Resistant
(n=44)
Sensitive
(n=16)

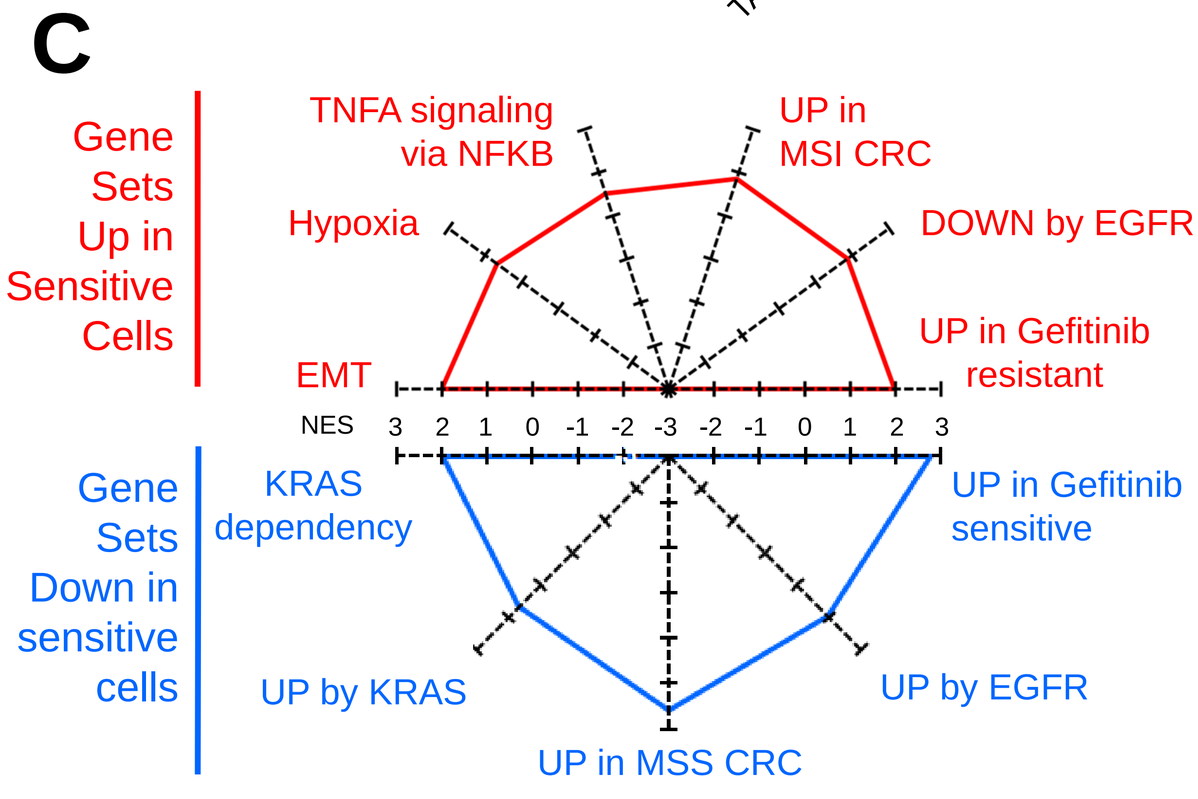
C
Gene Sets Up in Sensitive Cells
Gene Sets Down in sensitive cells
TNFA signaling via NFKB
UP in MSI CRC
Hypoxia
DOWN by EGFR
UP in Gefitinib resistant
EMT
NES
3 2 1 0 -1 -2 -3 -2 -1 0 1 2 3
KRAS dependency
UP in Gefitinib sensitive
UP by KRAS
UP by EGFR
UP in MSS CRC

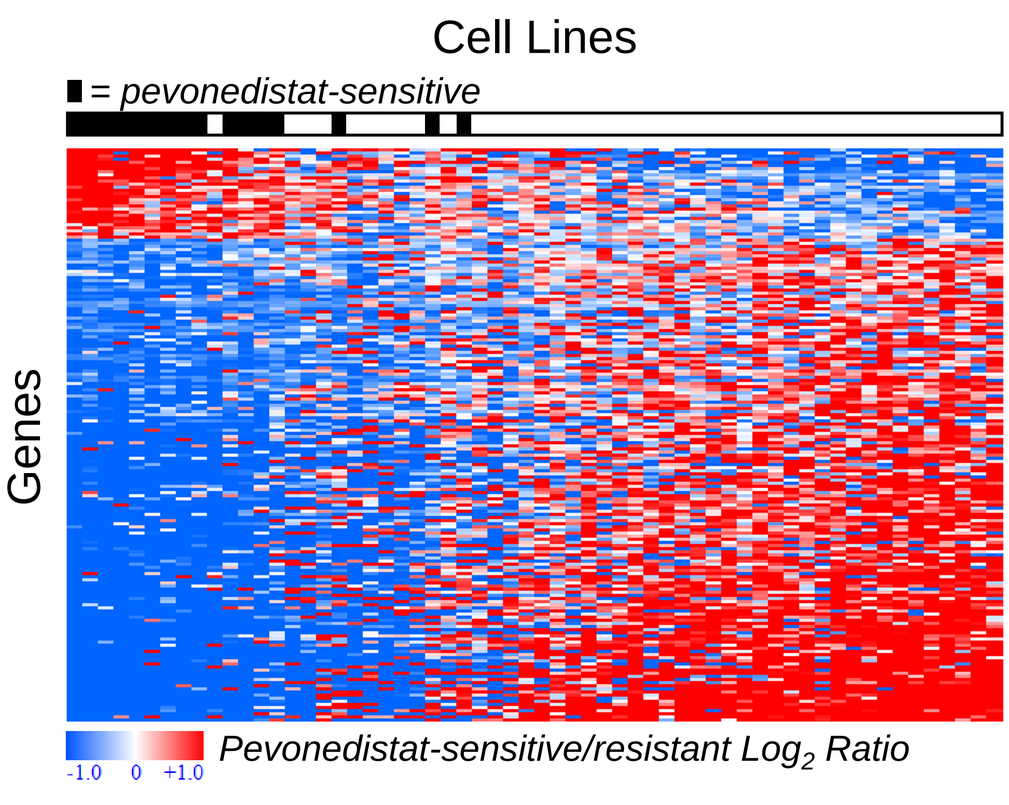
D
Cell Lines
= pevonedistat-sensitive
Genes
Pevonedistat-sensitive/resistant Log2 Ratio
-1.0
0
+1.0

A

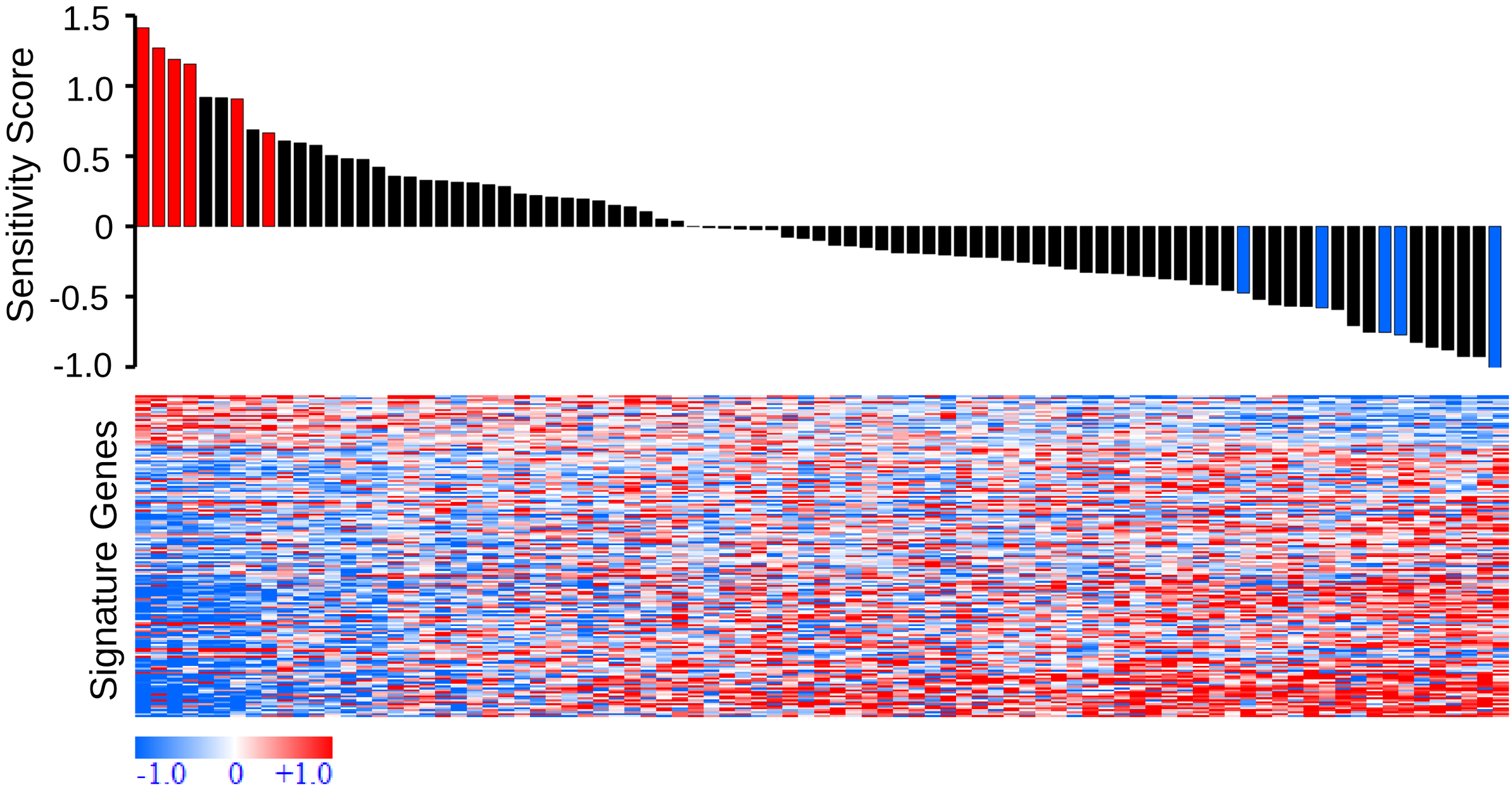
Sensitivity Score
1.5
1.0
0.5
0
-0.5
-1.0
Signature Genes
-1.0 0 +1.0

B

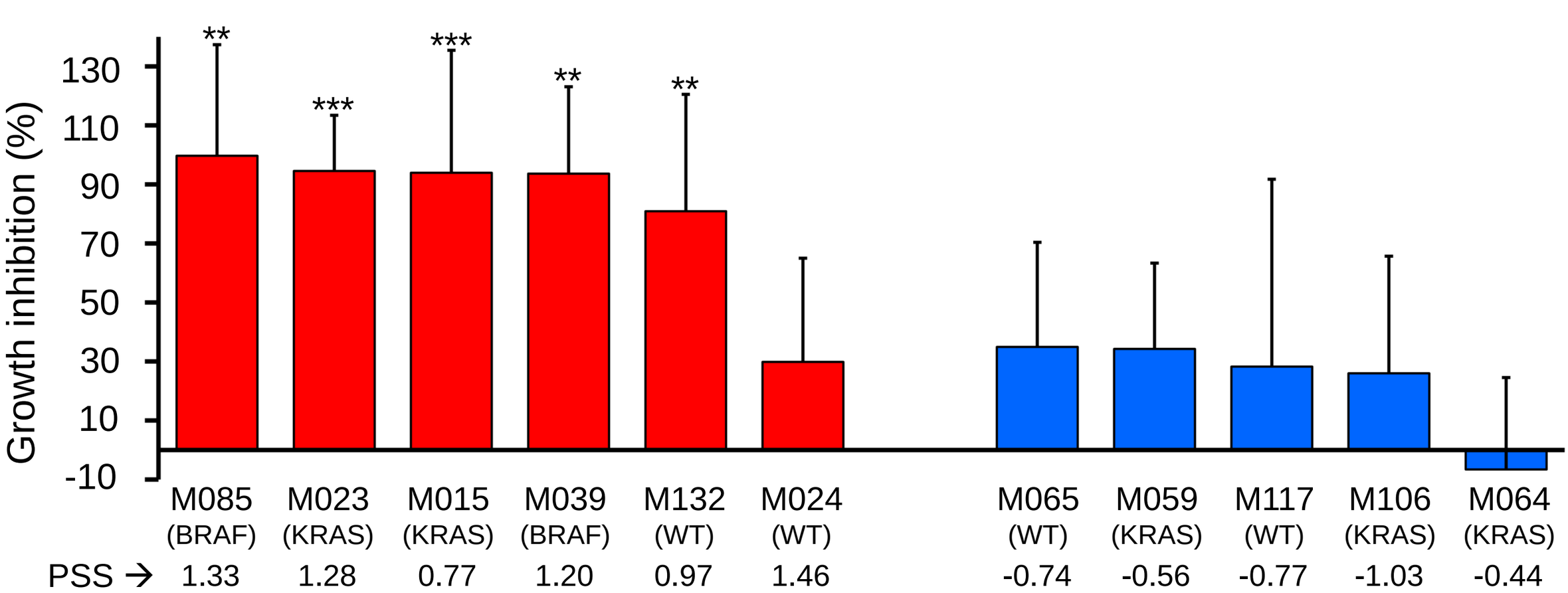
Growth inhibition (%)
130
110
90
70
50
30
10
-10
**
***
***
**
**
M085 (BRAF)
M023 (KRAS)
M015 (KRAS)
M039 (BRAF)
M132 (WT)
M024 (WT)
M065 (WT)
M059 (KRAS)
M117 (WT)
M106 (KRAS)
M064 (KRAS)
PSS →
1.33
1.28
0.77
1.20
0.97
1.46
-0.74
-0.56
-0.77
-1.03
-0.44

C

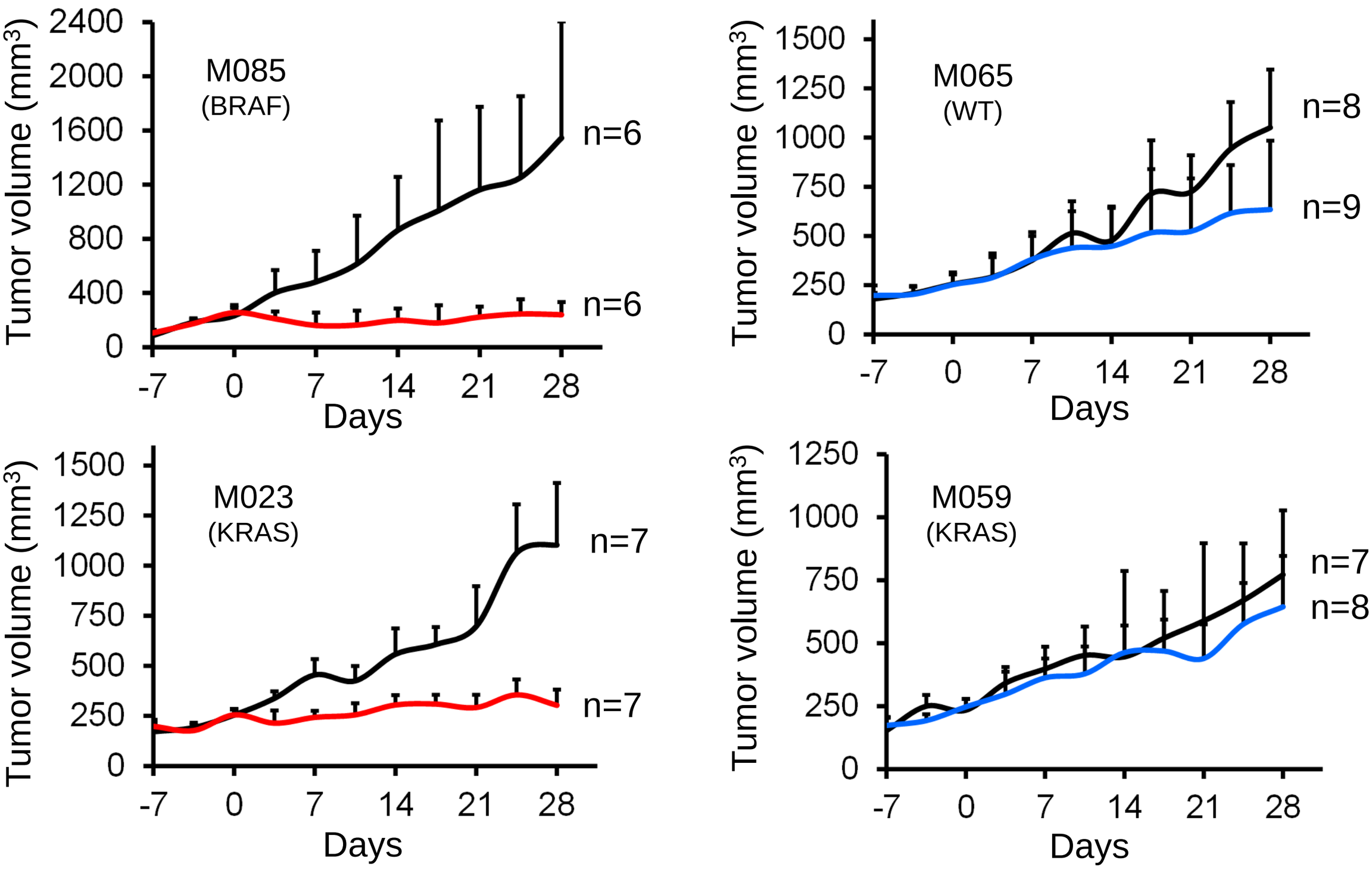
Tumor volume (mm³)
M085 (BRAF)
n=6
n=6
M065 (WT)
n=8
n=9
M023 (KRAS)
n=7
n=7
M059 (KRAS)
n=7
n=8
-7
0
7
14
21
28
Days

A

M085

P < .001

Ki67-positive nuclei (%area)

75
50
25
0

Vehicle
Pevo

Vehicle

Pevo

M065

Vehicle

Ki67-positive nuclei (%area)

45
30
15
0

Vehicle
Pevo

Pevo

B

M085

P < .001

P21-positive nuclei (%area)

60
40
20
0

Vehicle
Pevo

Vehicle

Pevo

M065

Vehicle

P21-positive nuclei (%area)

45
30
15
0

Vehicle
Pevo

Pevo

C

M085

P <.001

P27-positive nuclei (%area)

45
30
15
0

Vehicle
Pevo

Vehicle

Pevo

M065

Vehicle

P27-positive nuclei (%area)

45
30
15
0

Vehicle
Pevo

Pevo

A

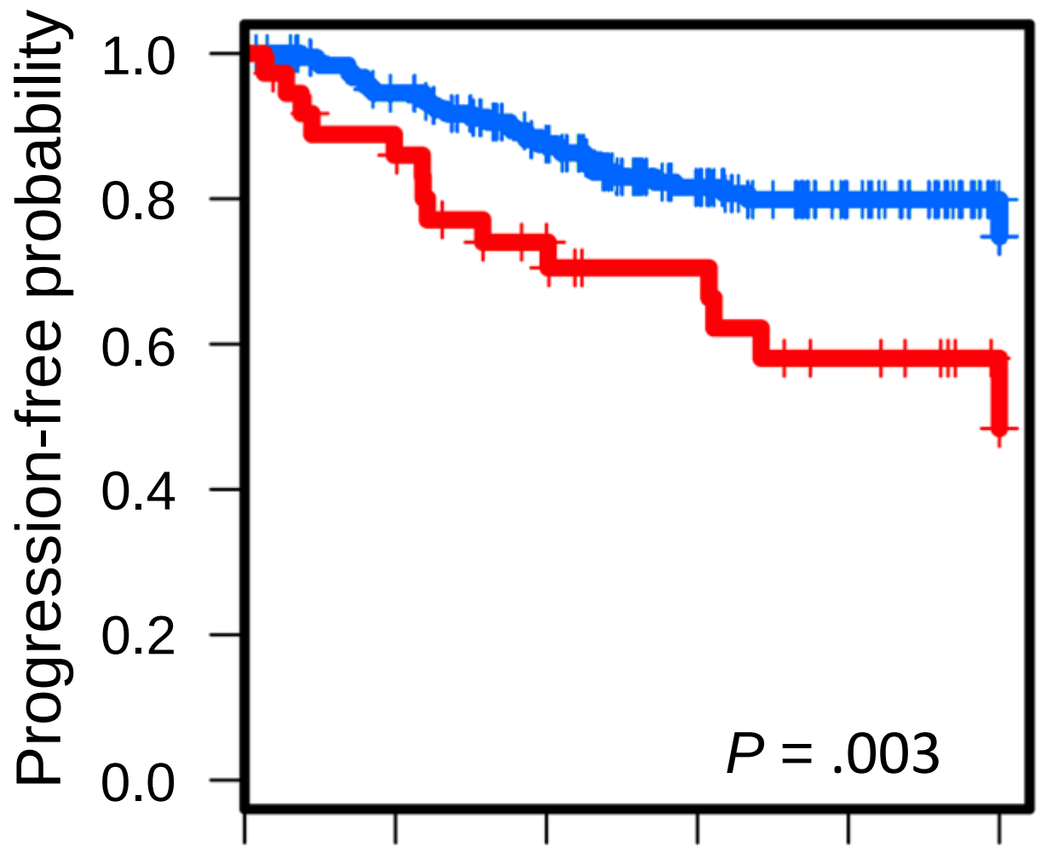

Years	0	1	2	3	4	5
	189	171	142	108	77	47
	37	30	22	17	12	6

B

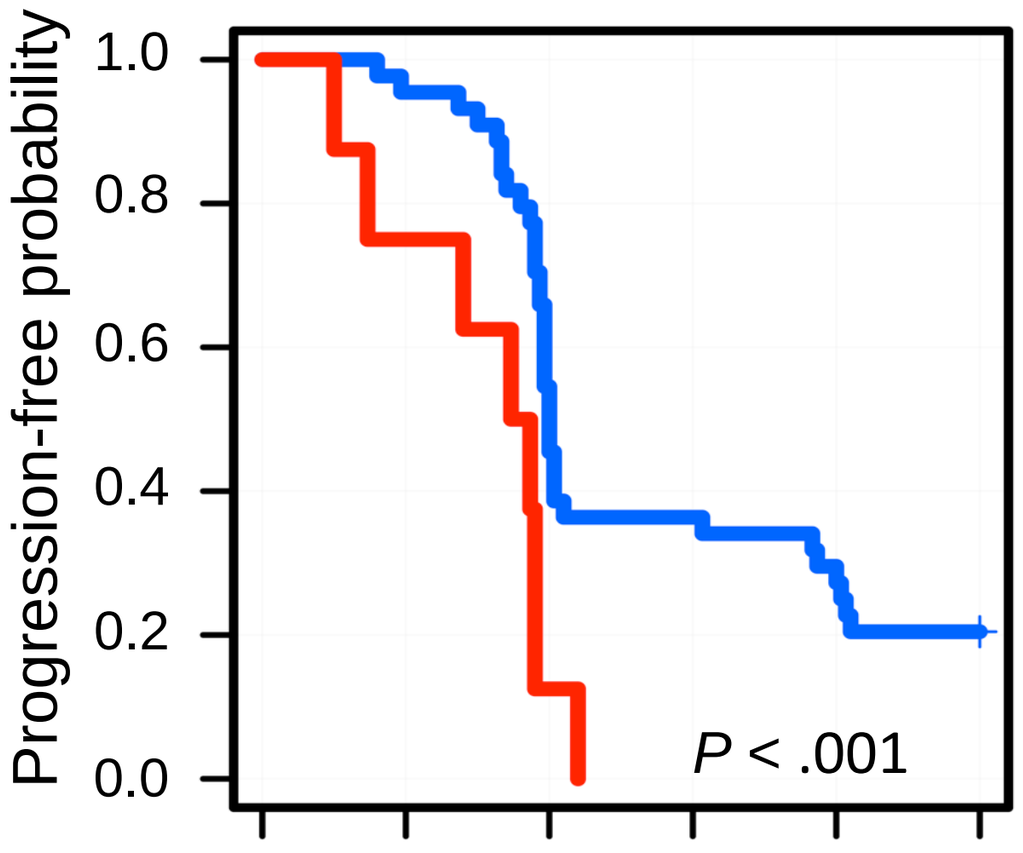

Days	0	30	60	90	120	150
	44	42	24	16	13	9
	8	6	1			

C

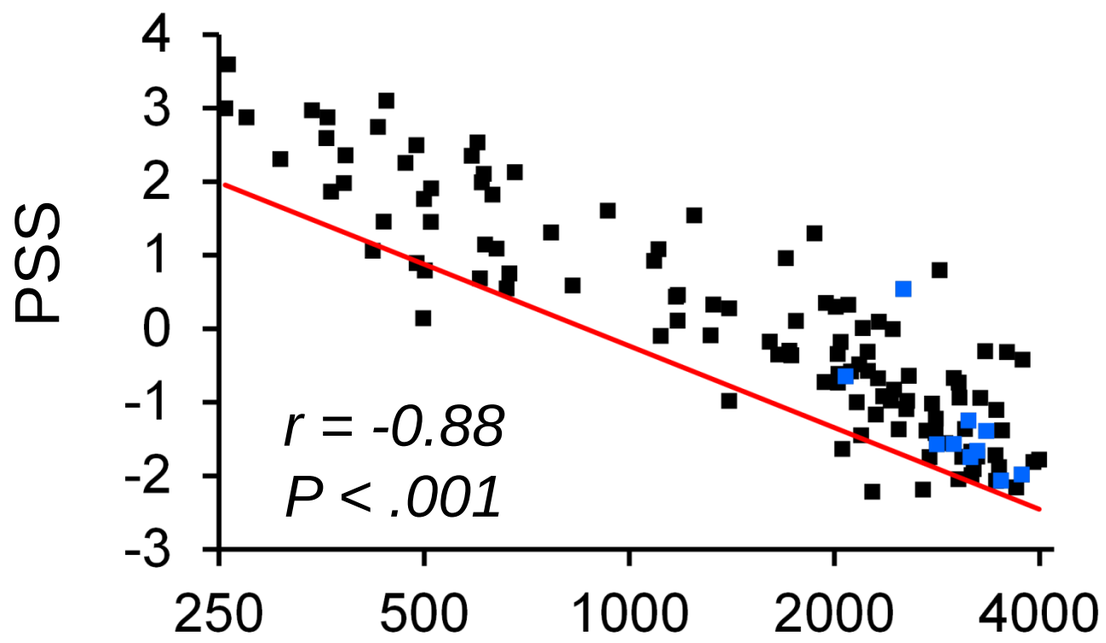

D

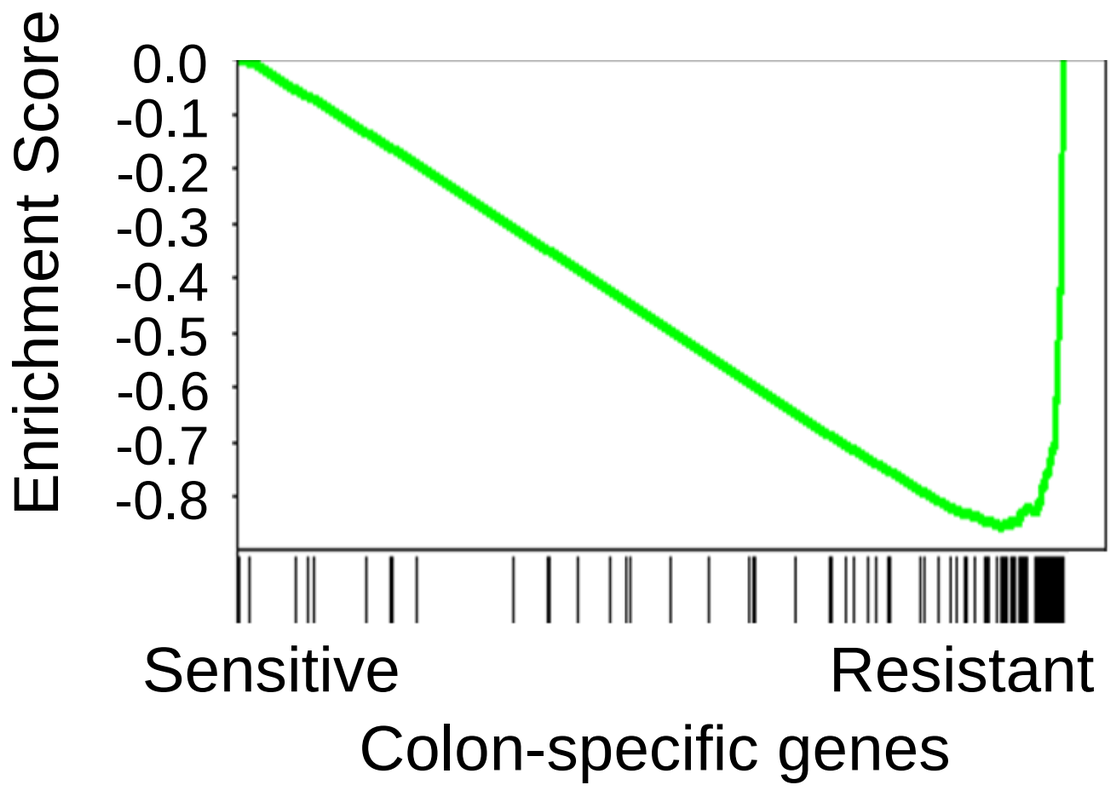

E

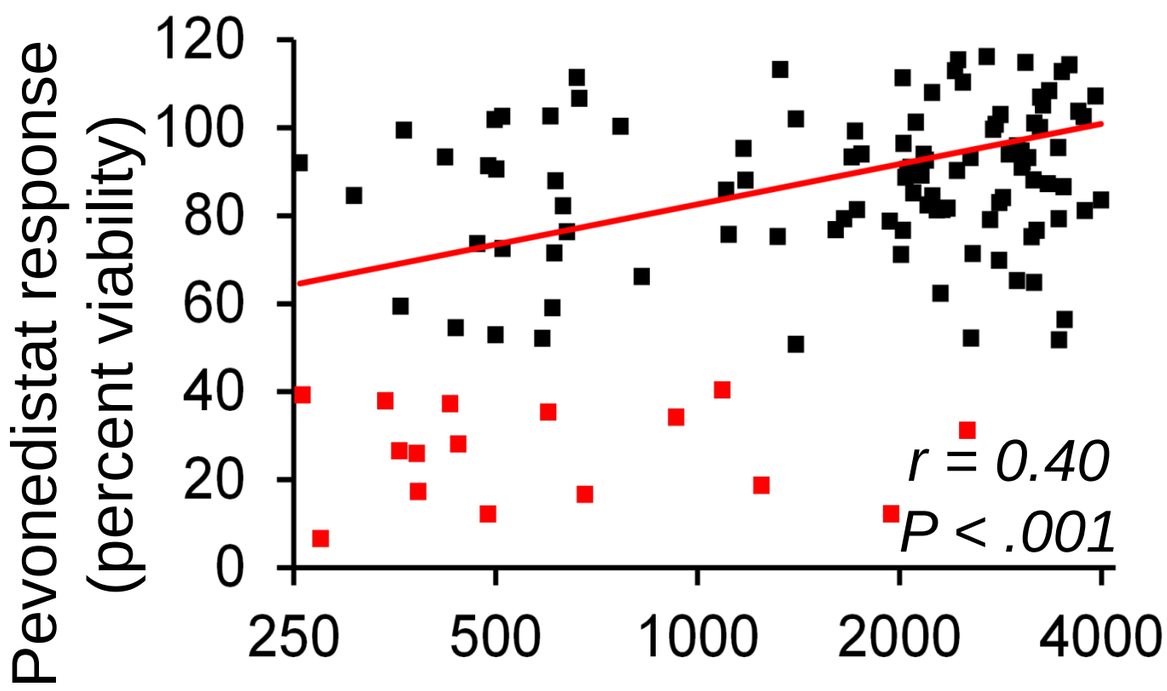

F

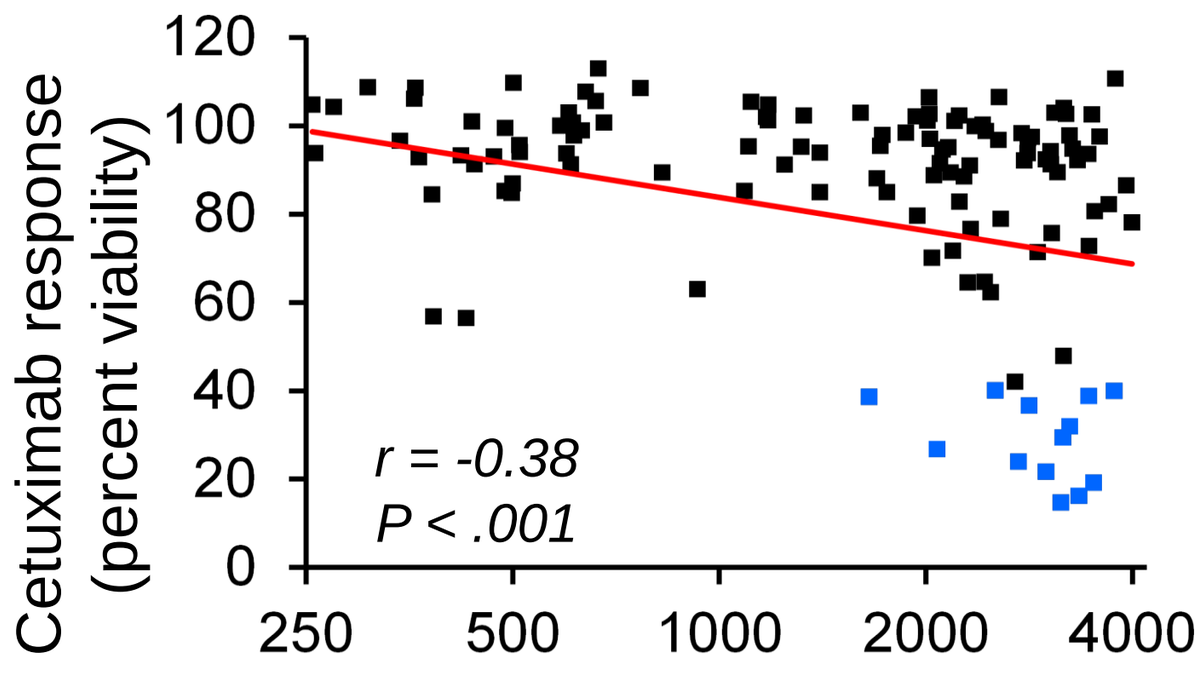

G

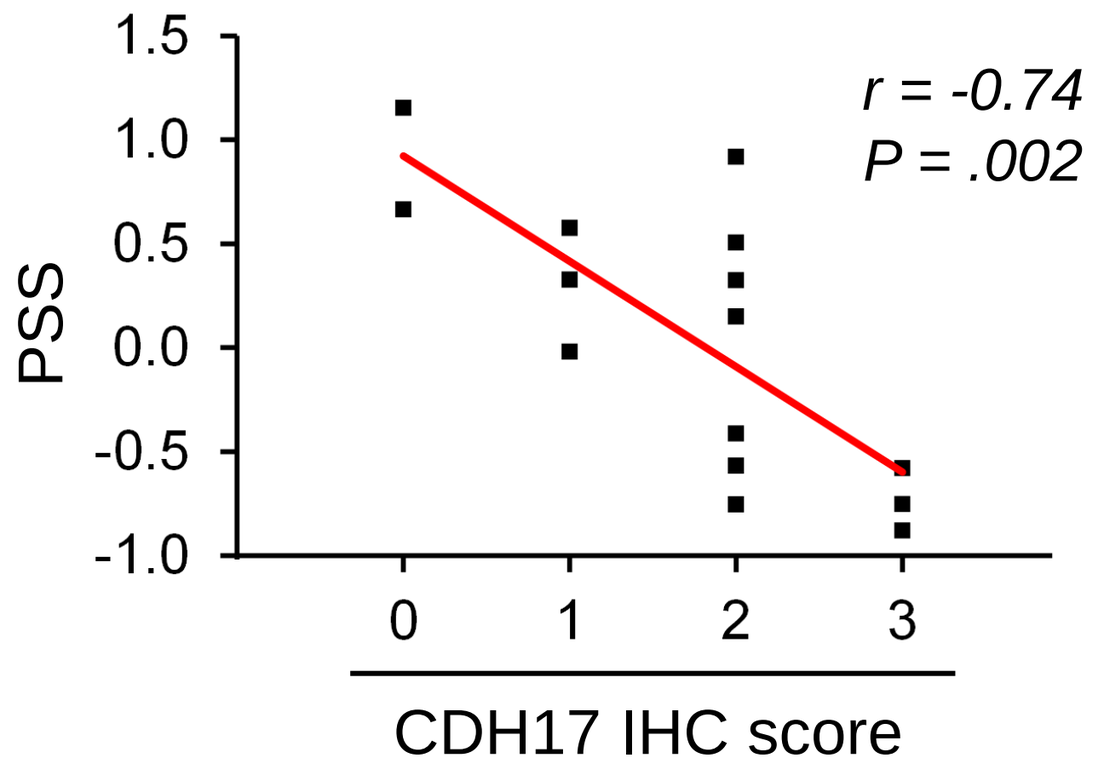

H

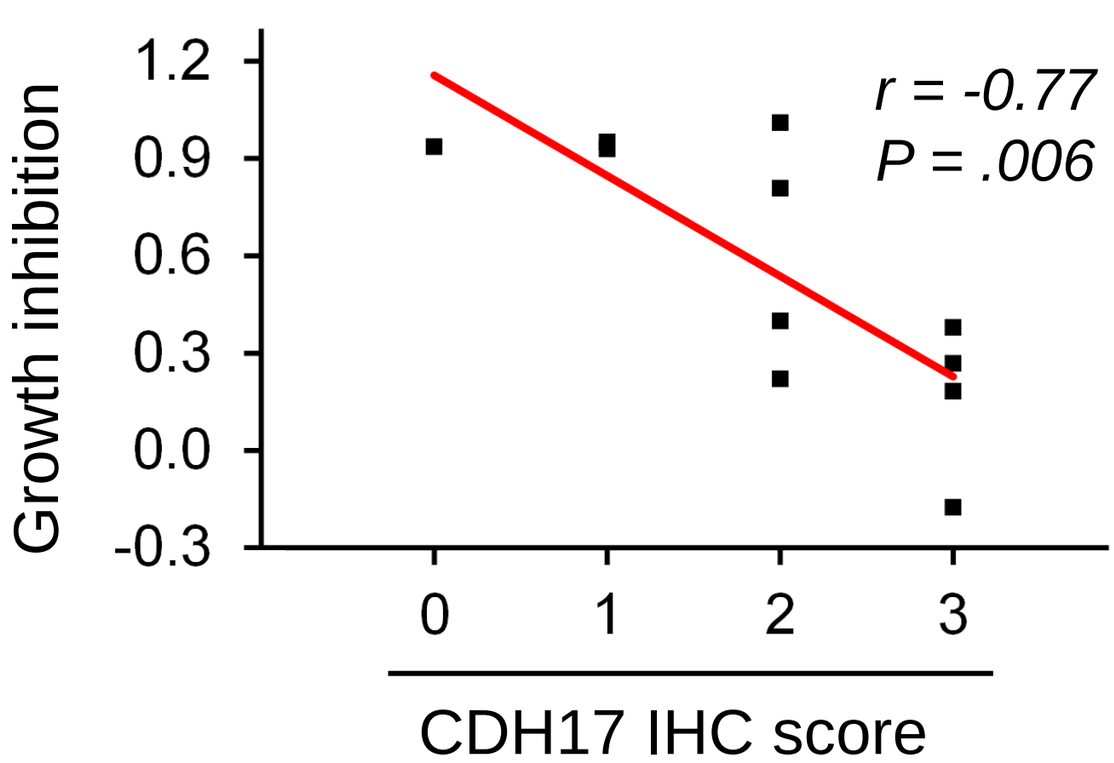

A

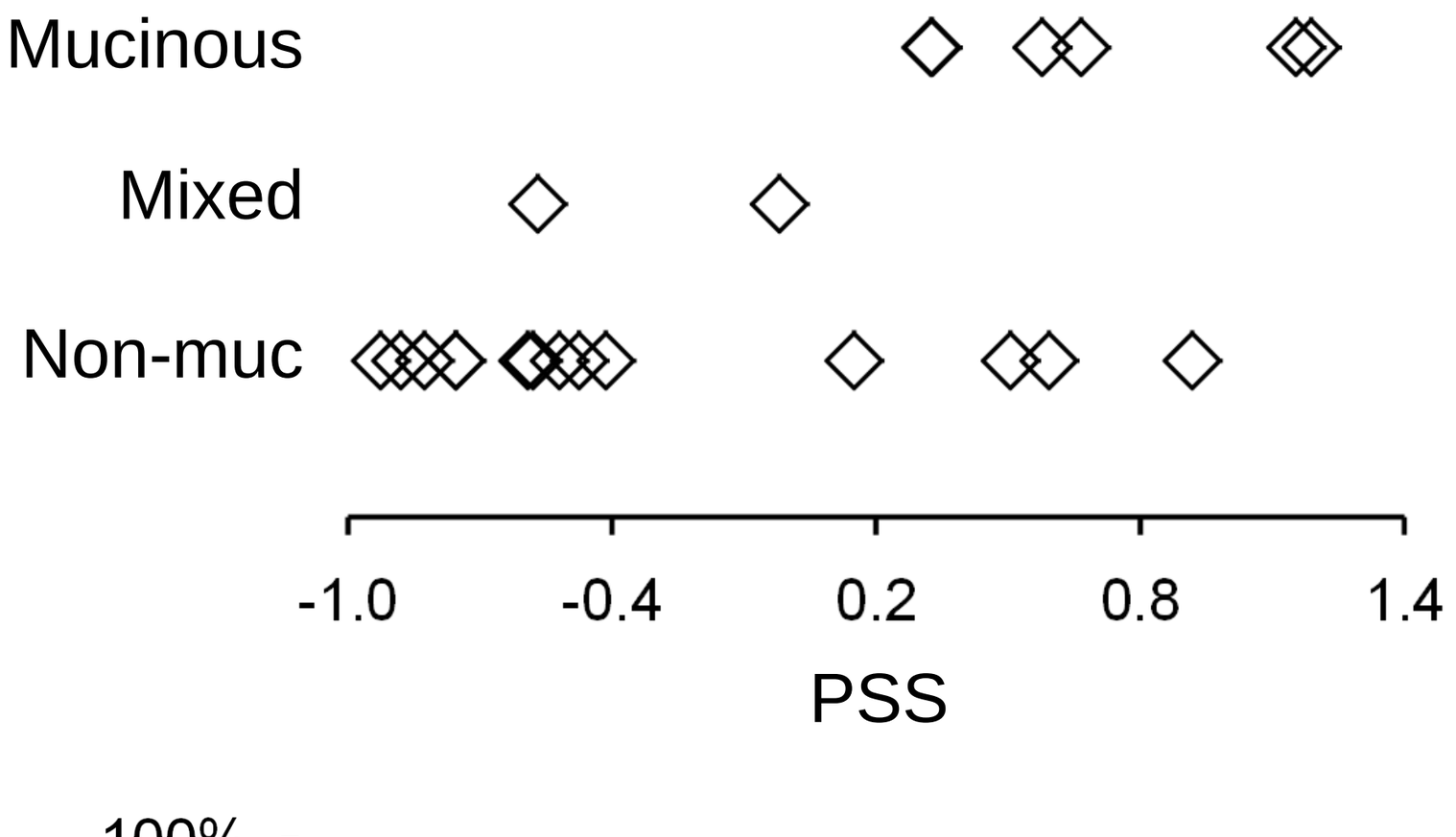

B

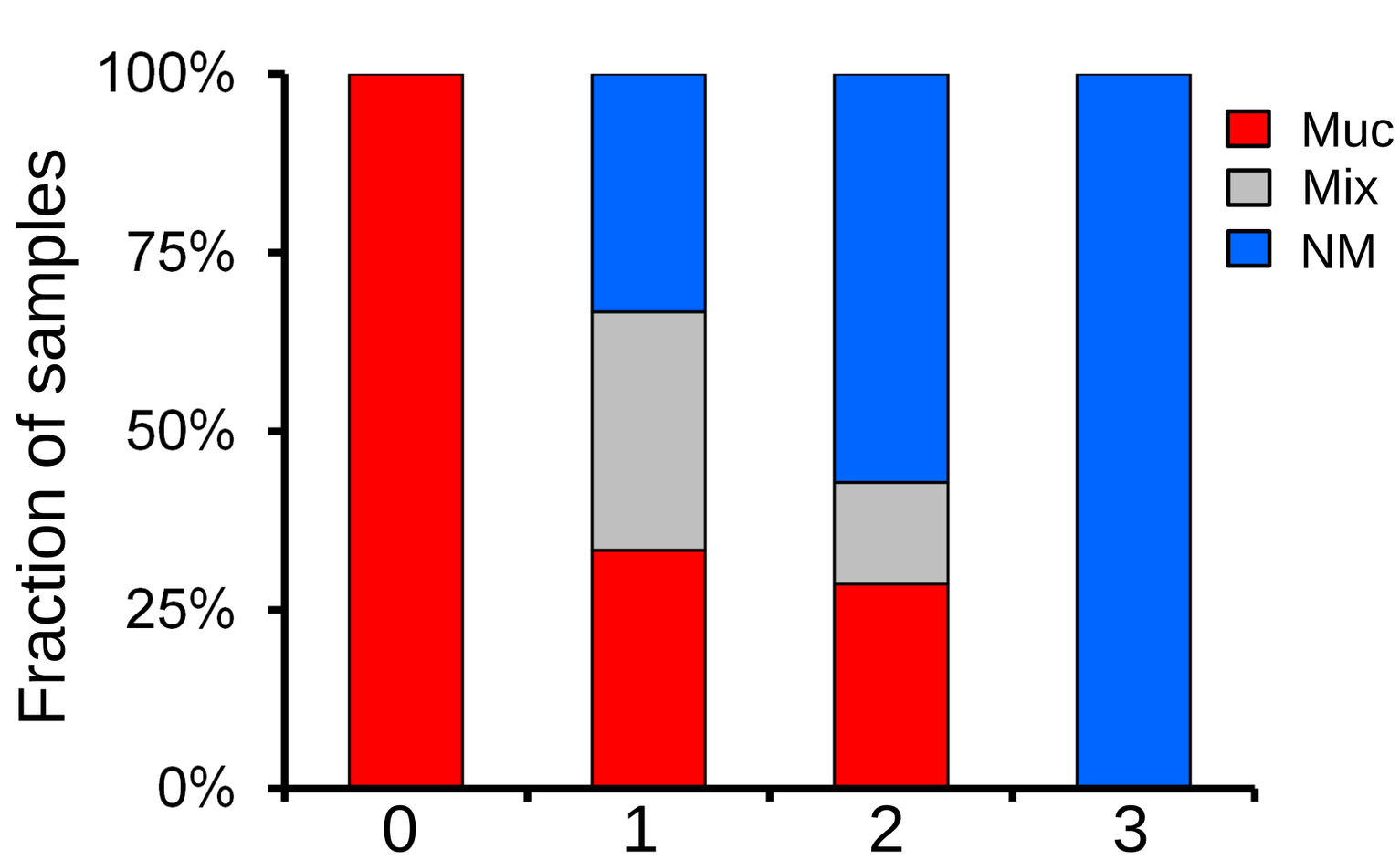

C pevonedistat-sensitive

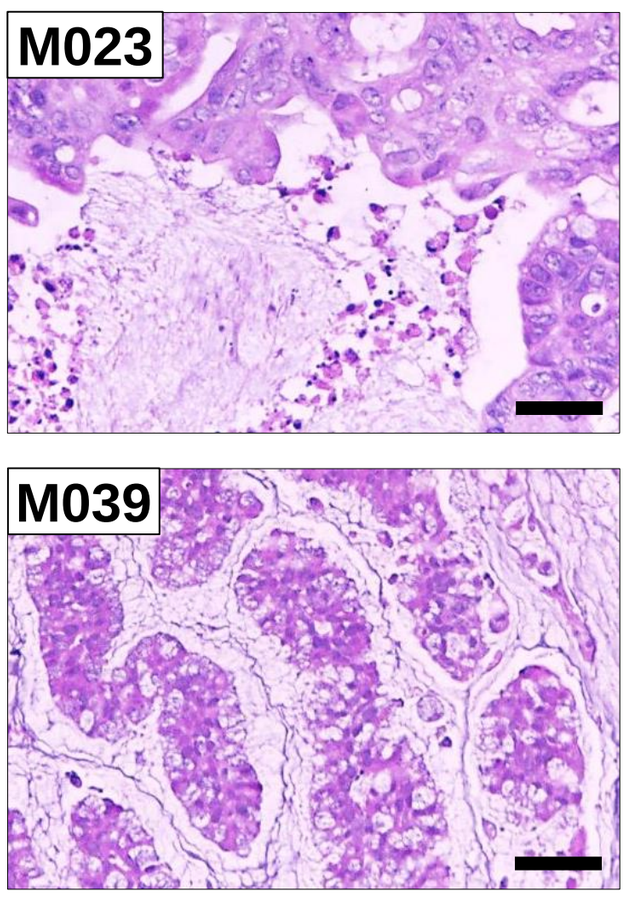

D pevonedistat-resistant